Protein palmitoylation-mediated palmitic acid sensing causes blood-testis barrier damage via inducing ER stress

Xie Ge [a,1], Zhaowanyue He [a,1], Chun Cao [b,1], Tongmin Xue [c], Jun Jing [a], Rujun Ma [a], Wei Zhao [a], Ling Liu [d], Kadiliya Jueraitetibaike [a], Jinzhao Ma [a], Yuming Feng [a,b], Zhang Qian [a], Zhichuan Zou [a], Li Chen [a], Chuanhai Fu [d,**], Ninghong Song [e,***], Bing Yao [a,c,*]

[a] Department of Reproductive Medical Center, Jinling Hospital, Nanjing University, School of Medicine, Nanjing, 210002, Jiangsu, China
[b] The First School of Clinical Medicine, Southern Medical University, Nanjing, 210002, Jiangsu, China
[c] State Key Laboratory of Reproductive Medicine, Nanjing Medical University, Nanjing, 210029, Jiangsu, China
[d] CAS Center for Excellence in Molecular Cell Sciences, Ministry of Education Key Laboratory for Membrane-less Organelles & Cellular Dynamics, Hefei National Laboratory for Physical Sciences at the Microscale, School of Life Sciences, Division of Life Sciences and Medicine, University of Science and Technology of China, Hefei, 230027, Anhui, China
[e] Department of Urology, The First Affiliated Hospital of Nanjing Medical University, Nanjing, 210000, Jiangsu, China

A R T I C L E   I N F O

A B S T R A C T

Blood-testis barrier (BTB) damage promotes spermatogenesis dysfunction, which is a critical cause of male infertility. Dyslipidemia has been correlated with male infertility, but the major hazardous lipid and the underlying mechanism remains unclear. In this study, we firstly discovered an elevation of palmitic acid (PA) and a decrease of inhibin B in patients with severe dyszoospermia, which leaded us to explore the effects of PA on Sertoli cells. We observed a damage of BTB by PA. PA penetration to endoplasmic reticulum (ER) and its damage to ER structures were exhibited by microimaging and dynamic observation, and consequent ER stress was proved to mediate PA-induced Sertoli cell barrier disruption. Remarkably, we demonstrated a critical role of aberrant protein palmitoylation in PA-induced Sertoli cell barrier dysfunction. An ER protein, Calnexin, was screened out and was demonstrated to participate in this process, and suppression of its palmitoylation showed an ameliorating effect. We also found that ω-3 poly-unsaturated fatty acids down-regulated Calnexin palmitoylation, and alleviated BTB dysfunction. Our results indicate that dysregulated palmitoylation induced by PA plays a pivotal role in BTB disruption and subsequent spermatogenesis dysfunction, suggesting that protein palmitoylation might be therapeutically targetable in male infertility.

1. Introduction

Infertility is becoming a nonnegligible problem in the modern world, and male infertility contributes to 30%–50% the infertile cases [1,2]. Spermatogenesis dysfunction is a critical cause of male infertility. In the spermatogenic microenvironment, Sertoli cell is the only somatic cell that directly interacts with germ cells, and is vital for spermatogenesis by supporting germ cells structurally and nutritionally. Sertoli cells form the blood-testis barrier (BTB), which provides an immune-privileged microenvironment for spermatogenesis and protects germ cells against harmful influences. Tight junction is a major junctional component of the BTB, and its integrity is critical for normal spermatogenesis [3,4].

Dyslipidemia is one of the contributing factors to male infertility, and a disruption of BTB may be involved [5,6]. Identification of the pivotal lipid component involved in this process and clarification of the underlying mechanism can further our understanding and treatment of male infertility. Dyslipidemia is often accompanied with abnormal levels of fatty acids, especially saturated fatty acids (SFAs) [7]. Palmitic acid (PA; C16:0) is the most frequent SFA in food as well as the most abundant circulating SFA. An increase of circulating PA is associated

with the incidence of the complications of dyslipidemia [8]. However, whether spermatogenesis dysfunction is associated with a higher PA level in the circulatory system remains unclear.

We previously reported that PA is lipotoxic to Sertoli cells [9,10]. Therefore, PA may affect Sertoli cell functions and the spermatogenic microenvironment, but the relevant mechanism needs further research. Endoplasmic reticulum (ER) is the largest organelle in mammalian cells, and accumulation or aggregation of misfolded proteins in ER induces ER stress. Both dyslipidemia and saturated fatty acids have been reported to be associated with ER stress, which can induce cellular dysfunction in various cell types [11,12]. ER stress activates the unfolded protein response (UPR), which is linked to the production of reactive oxygen species (ROS), and these biological processes instigate each other to disrupt cellular homeostasis [13]. ER stress has also been reported to regulate barrier integrity [14]. Thus we investigated whether PA induces barrier disruption and ER stress in Sertoli cells.

PA acts not only as an energy source, but also as a signaling molecule. At the posttranslational level, PA can act as a substrate for protein modification via the formation of thioester bonds in a process called palmitoylation (or *S*-palmitoylation), which regulates the functions of numerous proteins. Regarding ER, palmitoylation modulates ER proteostasis, ER-mitochondria-calcium crosstalk, ER protein enrichment on mitochondria-associated membranes, protein transport from the ER to the Golgi apparatus and cytomembrane, and tethering of the ER to the plasma membrane, all of which affect the functions of the ER [15–18]. On the other hand, because PA is the most abundant substrate, changes in PA concentrations may dysregulate palmitoylation [19,20], which could be involved in PA-induced Sertoli cell dysfunction. The involvement of palmitoylation in the regulation of Sertoli cell functions and the spermatogenetic microenvironment has never been well studied before, and the relevant research will provide a new direction for the treatment of male infertility.

In the present study, we identified elevated PA levels in the serum of patients with severe spermatogenetic dysfunction. Based on this result, we explored the effects of PA on BTB and the tight junctions formed by Sertoli cells. The involvement of ER stress was also investigated by subcellular distribution of PA, ultrastructural observation by electron microscopy, and dynamic observation of ER. In addition, we confirmed the involvement of palmitoylation in this process, and identified an ER protein Calnexin (CNX) as a critical palmitoylated protein. We explored the effects of ω-3 polyunsaturated fatty acids (PUFAs) on PA-induced Sertoli cell dysfunction and on protein palmitoylation. Our findings suggest that abnormal palmitoylation in Sertoli cells contributes to Sertoli cell barrier disruption and spermatogenesis dysfunction, which provides insights to pathogenesis and treatment of male infertility accompanied with dyslipidemia.

2. Results

2.1. Serum PA levels are significantly higher in patients with severe dyszoospermia

Aiming to understand the possible relationship between fatty acid constitution and spermatogenesis dysfunction, severe spermatogenesis dysfunction, including non-obstructive azoospermia (NOA) and extreme oligospermia (EO), was selected for our clinical analysis. To be specific, serum samples from 25 patients with NOA (n = 22) or EO (n = 3) and 25 healthy individuals (controls) were collected for fatty acid composition analysis (Table S1, Table S2). Quantification of 39 medium- and long-chain free fatty acids (C6–C24) was executed using gas chromatography coupled to mass spectrometry (GC/MS). According to the result, the levels of total medium and long-chain fatty acid (MLCFA) content were elevated in the patients, accompanied by significantly increased saturated, but not unsaturated fatty acids (Fig. 1A–C). Also, the ratio between SFA and unsaturated fatty acid (USFA), i.e. SFA/USFA, showed a significant increase (Fig. 1D). PA (C16:0) was the major component, comprising 63.80% of the serum SFAs (Fig. 1E). The significantly elevated serum PA levels in the patients with severe dyszoospermia (NOA and EA) (Fig. 1F) indicated a relationship among excess PA and disturbed spermatogenesis.

As an important hormone produced by Sertoli cells, inhibin B (INHB) showed a significant decrease in the serums of patients with NOA or EO, indicating that a dysfunction of Sertoli cells happened in these patients (Fig. 1G, Table S1). Combining with our fatty acid analysis results, we infer that a relationship may exist between excess PA and Sertoli cell dysfunction.

2.2. PA induces spermatogenesis dysfunction and blood-testis barrier disruption

To explore the effects of PA on spermatogenesis and Sertoli cell functions, we administered mice with PA by intraperitoneal injection
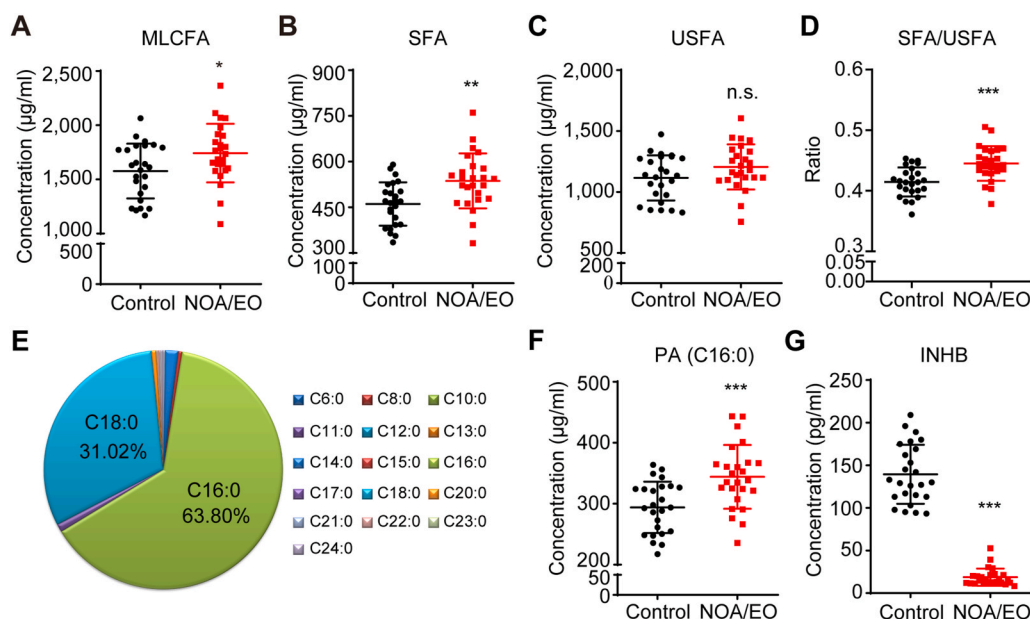

Fig. 1. Serum PA levels are significantly higher in patients with NOA or EO. (A–C) MLCFA (A), SFA (B), and USFA (C) levels in serums from patients were quantified using GC-MS. **(D)** The ratios between SFA and USFA levels in serums from patients were calculated. **(E, F)** SFA components (E) and PA levels (F) in serums from patients were quantified using GC-MS. **(G)** INHB levels in serums from patients were determined using chemiluminescence. Control, healthy controls (n = 25); NOA/EO, patients with NOA (n = 22) or EO (n = 3). Data are presented as mean ± SD. n. s., no significant difference vs. Control group. *$P < 0.05$, **$P < 0.01$, and ***$P < 0.001$ vs. Control group.

(Figs. 2 and S1). After 30 days of PA administration, sperm concentration and sperm motility were significantly decreased (Fig. 2A and B), although the body weight, testis weight and epididymis weight were not affected (Fig. S1). Hormone analysis indicated that INHB, which reflects Sertoli cell functions, showed a significant decline in the serum of PA treated mice (Fig. 2C). This result indicates that damage in the microenvironment of spermatogenesis may occur, and Sertoli cells are probably a critical target. Thus we observed BTB in testes. In fluorescein isothiocyanate isomer I (FITC-I) permeability assay, fluorescence was detected only in the interstitial portion and the basal lines of the seminiferous tubules in the testes of control mice, but was also observed in the lumen of the seminiferous tubules in the testes of mice injected with PA (Fig. 2D). Moreover, according to the TEM analyses of testes, the BTB of control mice was continuous and clearly delimited, while the BTB of mice administered with PA appeared discontinuous and loose (Fig. 2E). These observations indicate that BTB was severely destroyed by PA administration.

We also assessed the integrity of the Sertoli cell barrier in primary mouse Sertoli cells and TM4 Sertoli cells *in vitro*. Transepithelial resistance (TER) and FITC-dextran permeability assays revealed that PA impaired the cell barrier (Figs. 3A, 3B, S2A and S2B). PA also down-regulated the tight junction proteins zona occluden-1 (ZO-1), occludin (OCLN), claudin 11 (CLDN11) and claudin 5 (CLDN5) (Fig. S2C), implying that PA impaired tight junctions between Sertoli cells.

2.3. PA enters the ER and induces ER stress in Sertoli cells

In order to understand the mechanism underlying the disruption of Sertoli cell barriers by PA, we explored whether PA enters Sertoli cells and the exact organelle PA penetrated. We traced PA endocytosis into Sertoli cells using the green fluorescent PA analog BODIPY® FL C16.
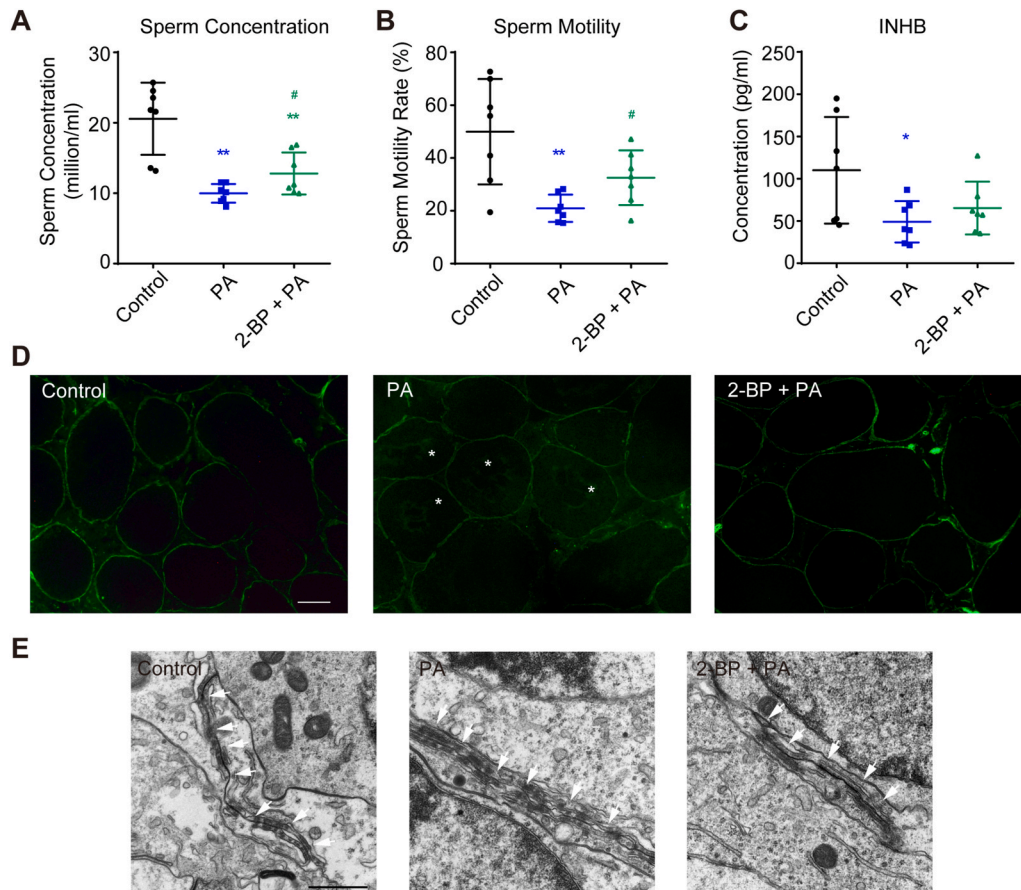
Fluorescence emission was detected in TM4 Sertoli cells after 30 min and the intensity increased over time (Fig. S2D), indicating that PA penetrates Sertoli cells. We analyzed the subcellular location of PA using BODIPY® FL C16, and lipid droplets, ER, and mitochondria were stained with Nile Red, ER-Tracker Red, and MitoRed, respectively. PA colocalized with lipid droplets and ER, but not mitochondria (Fig. 3C and D and S2E). Because lipid droplets store neutral lipids that function as energy sources and are not usually harmful, and lipid droplets arise from the ER [21], we further investigated the role of PA in the ER.

Electron microscopy revealed that the ER morphology in the PA group, showing widely dilated membranes with enlarged spaces, considerably differed from that of the control cells (Fig. 3E). Using ER tracker to stain ER in Sertoli cells, we found that in normal cells ER distributed in the cytoplasm with some reticular structures stained brighter at the periphery of nuclei. After 30 min of PA treatment, ER showed dispersed staining, and the reticular structures around nuclei disappeared (Fig. 3F). A sequential observation for 5 min revealed that the reticular structures around the nuclei kept intact dynamically in control cells (Video S1), while the structural failure was persistent in PA treated cells (Video S2). When the cells were treated with PA for 24 h, ER tracker staining was more obscure, and some punctate condensation appeared (Fig. 3G). These results indicate a severe damage of ER after PA treatment in Sertoli cells.

Moreover, the transcriptional expression levels of most ER stress markers, including glucose-regulated protein 78 (Grp78), C/EBP homologous protein (Chop), activating transcription factor 4 (Atf4), growth arrest and DNA damage-inducible transcript 34 (Gadd34), homocysteine-inducible endoplasmic reticulum stress-inducible ubiquitin-like domain member 1 protein (Herpud1), and hypoxia upregulated 1 (Hyou1), were upregulated in the PA group (Fig. S2F). Among these markers, Atf4 and Gadd34 are markers of the protein kinase R-like

Fig. 2. PA disrupts spermatogenesis, while 2-BP shows a rescuing effect. Mice were injected intraperitoneally (i.p.) with BSA (Control group) or PA-BSA (PA group) (n = 7 per group) once daily for 30 days, with or without gavage of 2-BP every two days. **(A, B)** Sperm concentrations (A) and sperm motilities (i.e. percentage of mobile sperms) (B) were assessed using a haemocytometer. **(C)** Concentrations of INHB in serums were analyzed by ELISA. Data are presented as mean ± SD. *$P < 0.05$ and **$P < 0.01$ vs. Control group. #$P < 0.05$ vs. PA group. **(D)** Assessment of BTB integrity *in vivo* using FITC-I permeability assays. Asterisks (*) indicate leaked FITC-I in the lumen of seminiferous tubules. Scale bars: 100 μm. **(E)** The ultrastructure of tight junctions was observed using transmission electron microscopy. White arrows indicate the tight junctions. Scale bars: 1 μm.
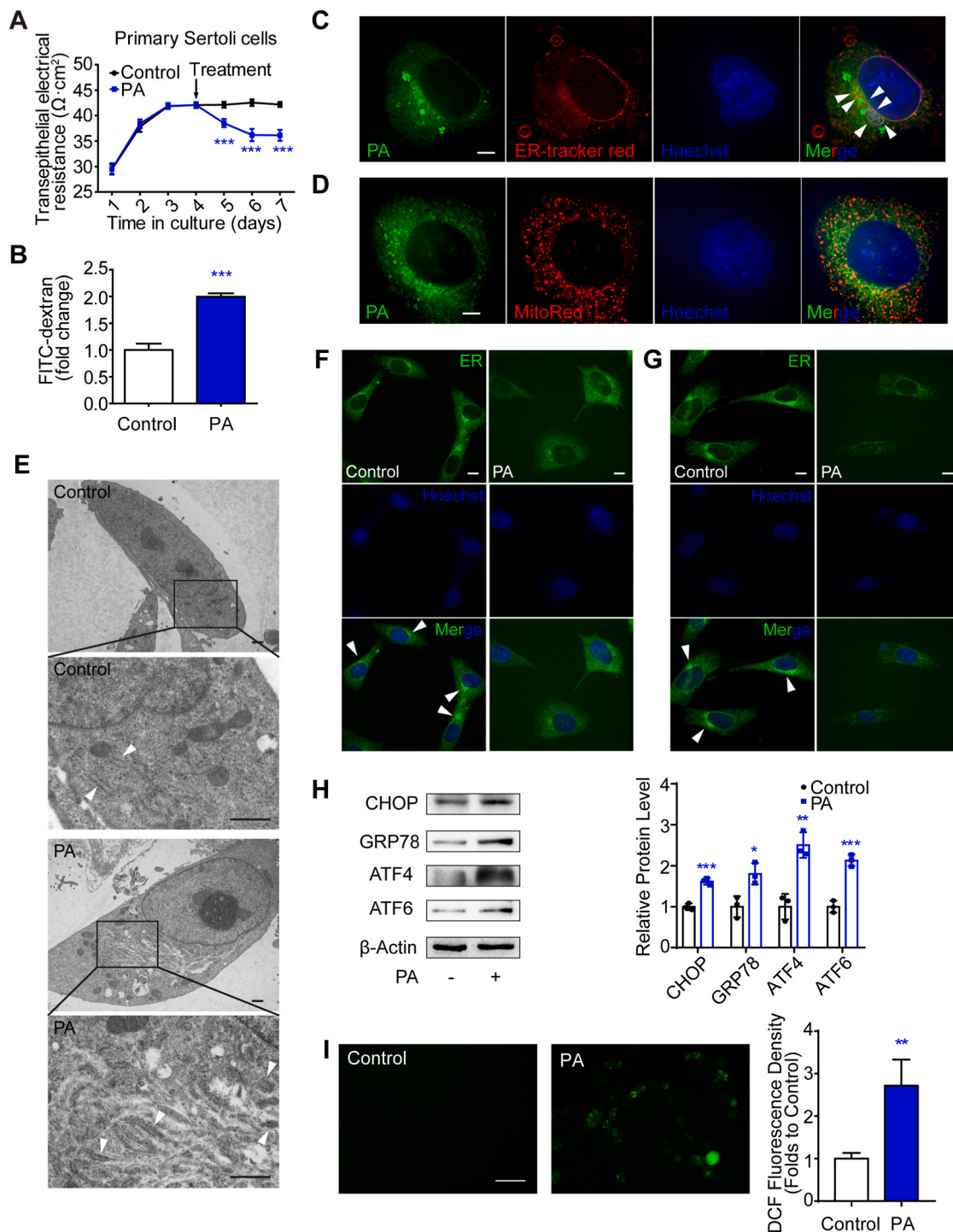
Fig. 3. PA damages cell barrier and induces ER stress in Sertoli cell. (A) TER detection of primary Sertoli cell barriers. The cells were incubated with (PA) or without (Control) 0.4 mM PA for 3 days after barriers were formed on day 4 (n = 5). **(B)** FITC-dextran permeability assessment of primary Sertoli cell barriers. The cells were treated with (PA) or without (Control) 0.4 mM PA for 24 h after cell barriers were formed (n = 5). **(C, D)** Subcellular localization of PA. Fluorescently marked PA (BODIPY® FL C16) colocalized with (C) ER (ER-Tracker Red), but not (D) mitochondria (MitoRed). The nuclei were stained with Hoechst. Scale bar: 5 μm. White arrowheads, PA and ER colocalization. **(E)** Ultrastructural changes in the ER of TM4 cells treated with (PA) or without (Control) 0.4 mM PA for 24 h were observed by transmission electron microscopy. The lower panels show magnifications of the boxed areas in the relevant upper panels, revealing ribosomes lining the ER membranes. Scale bar: 1 μm. **(F, G)** Observation of ER distribution in TM4 Sertoli cells by ER-Tracker Green staining. The cells were incubated with (PA) or without (Control) 0.4 mM PA for 30 min (F) or 24 h (G). The nuclei were stained with Hoechst. Scale bar: 10 μm. White arrowheads, reticular structures at the periphery of nuclei. Time-lapse observations of ER distribution were shown in the form of videos in Supplementary files (Video S1 and Video S2). **(H)** Translational expression levels of ER stress-related genes were analyzed using western blotting. The relative intensities of bands were quantified by ImageJ and normalized to β-actin levels (n = 3). **(I)** ROS detection using DCFH-DA staining. The fluorescence densities were calculated using ImageJ (n = 3). Scale bar: 50 μm. In Panels G and H, TM4 cells were incubated with (PA) or without (Control) 0.4 mM PA for 24 h. Data are presented as mean ± SD. *$P < 0.05$, **$P < 0.01$ and ***$P < 0.001$ vs. Control group. (For interpretation of the references to color in this figure legend, the reader is referred to the Web version of this article.)

endoplasmic reticulum kinase (PERK) signaling pathway, while Herpud1 and Hyou1 are markers of the ATF6 pathway. The protein expression levels of a critical ER chaperone GRP78, as well as the markers of PERK and ATF6 pathways, ATF4 and ATF6, were also up-regulated by PA (Fig. 3H). Conversely, PA did not alter the expression of the markers of the inositol-requiring enzyme 1 (IRE1) pathway, including X-box binding protein 1 (Xbp1; including total [Xbp1T] and spliced [Xbp1S] forms) and ER degradation-enhancing alpha-mannosidase like protein 1 (Edem) (Fig. S2F). Therefore, we concluded that PA activates the PERK and ATF6, but not the IRE1 pathway.

Since ER stress activation leads to ROS generation [22], we also detected ROS in Sertoli cells after PA treatment, and found that ROS generation was remarkably activated by PA (Fig. 3I). These findings indicate that PA causes ER stress in Sertoli cells.

2.4. ER stress signaling activation mediates PA-induced tight junction disruption in Sertoli cells

When TM4 Sertoli cells were incubated with the ER stress activator, tunicamycin (TM), the expression of ER stress marker genes were induced (Fig. S3A), confirming the activation of ER stress signaling. Assays of permeability using TER and FITC-dextran, as well as the analysis of tight junction protein expression levels, showed that TM induced cell barrier damage in Sertoli cells (Figs. S3B–F). Therefore, ER stress activation significantly disrupted tight junctions among Sertoli cells.

We have validated that PA activated PERK and ATF6 pathways, but not IRE1 pathway. Therefore, we used PERK inhibitor GSK2606414 and ATF6 inhibitor melatonin to treat Sertoli cells. Cell viability analysis showed that GSK2606414 and melatonin showed cytotoxicity at 10 nM and 10 μM, respectively (Fig. S3G). So we used concentrations up to the cytotoxic dose for cell survival rescuing analysis, and found that GSK2606414 showed most obvious rescuing effect at the concentration of 0.4 nM, while melatonin did not present any rescuing effect (Fig. S3H). We also observed an ameliorating effect of GSK2606414, but not of melatonin, on PA-induced Sertoli cell barrier disruption (Figs. S3I and S3J). These results indicate that activation of PERK pathway, rather than ATF6 pathway, is involved in PA-induced Sertoli cell barrier disruption.

CHOP is downstream of the PERK pathways, and is a critical component of ER stress signaling [23]. According to our results, PA significantly elevated CHOP expression in Sertoli cells not only on the transcriptional level, but also on the translational level (Figs. 3H and S2F). We also observed increase of CHOP expression after TM treatment (Figs. S3A and S4A). Since CHOP is a critical node between PERK pathway and cell damage, we furtherly investigated the effects of CHOP depletion using short interfering RNA (siRNA). As siCHOP obviously decreased CHOP expression (Figs. S4B and S4C), ROS generation, which was induced by PA, was evidently diminished (Fig. S4D), indicating a suppression of cell stress by CHOP RNA interfering (RNAi). Furthermore, siCHOP restored the levels of tight junction proteins that were decreased by PA (Fig. S4E), as well as the PA-disrupted Sertoli cell barriers, according to TER assays and FITC-dextran permeability assays (Figs. S4F and S4G). Therefore, PA induced the disruption of tight junctions in Sertoli cells by activating ER stress signaling.

2.5. PA activates ER stress signaling by inducing protein palmitoylation in Sertoli cells

Because PA is an important substrate in palmitoylation, we analyzed protein palmitoylation levels after PA treatment. In the testes of mice, we observed an up-regulation of palmitoylation level after PA injection (Fig. 4A), which indicate a possible involvement of protein palmitoylation in PA-induced testis toxicity. To furtherly determine the cell type affected in the spermatogenic microenvironment, we isolated primary cells in testes, including Sertoli, Leydig and germ cells, to detect the palmitoylation levels after PA treatment. As shown in Fig. 4B, PA induced palmitoylation most significantly in Sertoli cells, which prompts that Sertoli cells may be the cell type most sensitive to PA-induced palmitoylation in this microenvironment. In the TM4 Sertoli cell line, an increase of palmitoylation after PA treatment was also found (Fig. S5A). Combined with our previously identified fact that PA damages Sertoli cell functions, Sertoli cell was selected for further studies.
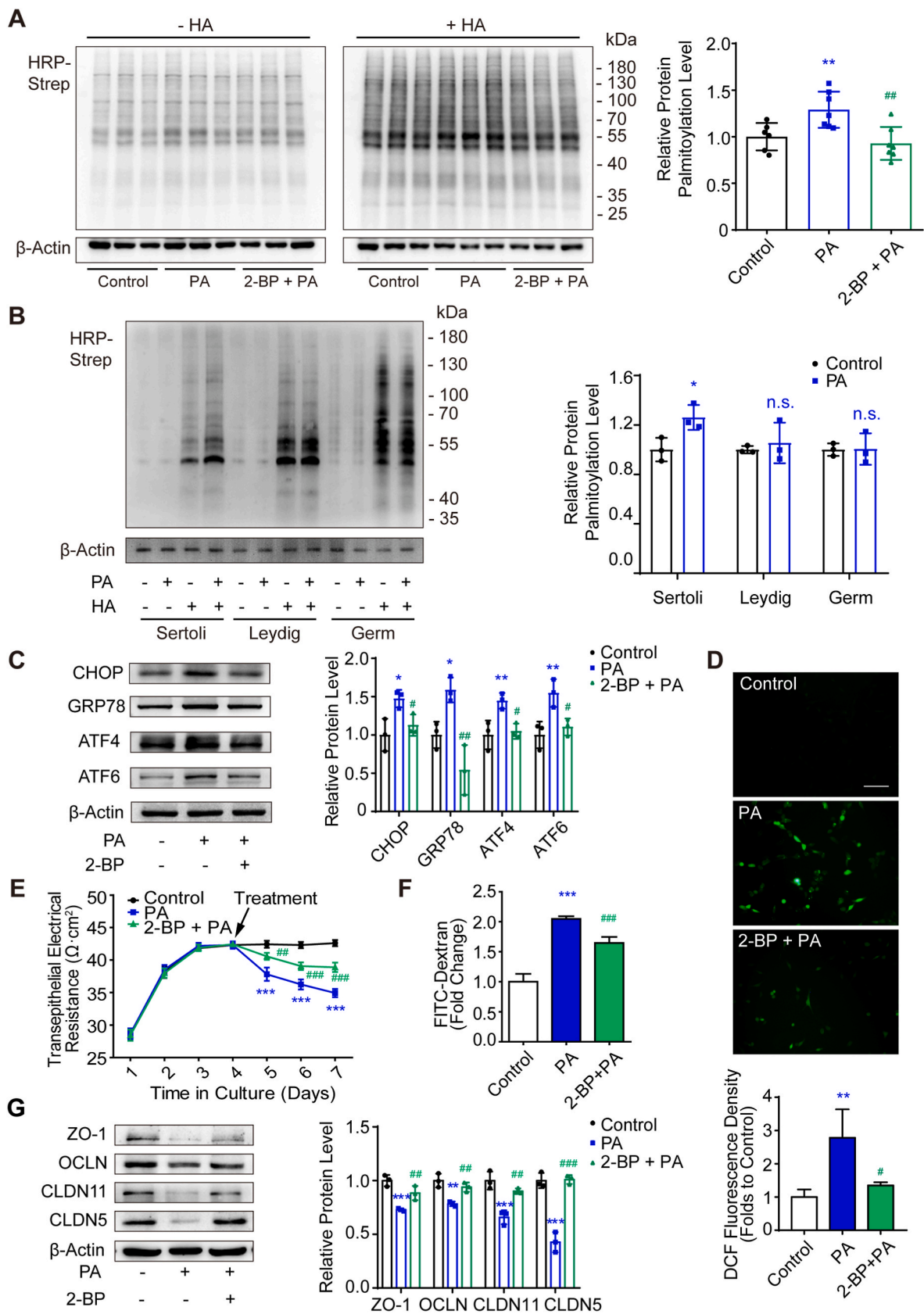
Using the palmitoylation inhibitor 2-bromopalmitate (2-BP, 10 μM), we suppressed PA-induced palmitoylation in Sertoli cells (Fig. S5A). Interestingly, prior incubation of Sertoli cells with 2-BP (5, 10, and 20 μM) substantially ameliorated PA-induced ER stress at an optimal concentration of 10 μM (Fig. S5B). The alleviation of PA-induced ER stress by 2-BP (10 μM) was furtherly confirmed by protein expression analysis of ER stress markers and ROS detection (Fig. 4C and D). These results indicated that palmitoylation is critical for PA-induced stress in the ER of Sertoli cells.

2.6. Inhibition of palmitoylation significantly ameliorates PA-induced spermatogenesis dysfunction and BTB disruption

We investigated whether protein palmitoylation plays a role in PA-induced Sertoli cell barrier disruption. Both TER and FITC-dextran permeability assays indicated that 2-BP protected primary mouse Sertoli cells and TM4 cells against PA-induced barrier destruction (Figs. 4E, 4F, S5C and S5D). The expression of TJP1, CLDN11, OCLN, and CLDN5, which was decreased by PA, was also rescued by 2-BP (Fig. 4G). These results further confirmed that palmitoylation is involved in PA-induced Sertoli cell dysfunction.

As a distribution balance of tight junction proteins between the membrane and the cytoplasm contributes to the integrity of cell barriers, we furtherly analyzed the expression of the tight junction protein OCLN on the membrane and in the cytoplasm of Sertoli cells. The result showed that OCLN decreased after PA treatment and increased after 2-BP rescuing in the membrane, but remained constant in the cytoplasm (Fig. S5E). Combined with the previous result that tight junction proteins showed lower expression after PA treatment and their expression recovered after 2-BP rescuing (Fig. 4G), we concluded that both PA and 2-BP may regulate tight junction proteins by modulating their expression on cell membrane but not in cytoplasm.

To investigate the effects of palmitoylation inhibition on spermatogenesis and BTB *in vivo*, we gavaged mice with 2-BP simultaneously to PA administration. Firstly, the palmitoylation inhibiting effects of 2-BP was proved by analyzing protein palmitoylation in mouse testes (Fig. 4A). Furtherly, as shown in Fig. 2A and B, 2-BP gavage significantly recovered sperm concentration and sperm motility, which were suppressed by PA. Hormone detection showed that both follicle-stimulating hormone (FSH) and luteinizing hormone (LH), which were two important sex hormones relating to spermatogenesis and were decreased by PA in this experiment, remained at low levels after 2-BP treatment (Figs. S1F and S1G), indicating that palmitoylation inhibition may not recover the hypothalamus–pituitary–gonadal axis *in vivo*. In one of our previously published studies, we used FSH as a representative hormone to treat HFD-fed mice with high PA levels, and demonstrated that spermatogenesis dysfunction induced by dyslipidemia is more possibly be induced by damage in the microenvironment rather than by the abnormal hormone levels [24]. Hence, the spermatogenic microenvironment may be a critical rescuing target of palmitoylation inhibition using 2-BP. According to our previous results, Sertoli cell may be the cell type most sensitive to PA-induced palmitoylation in the spermatogenic microenvironment. However, INHB level was not augmented by 2-BP (Fig. 2C). So we furtherly observed BTB, which reflects the barrier function of Sertoli cells. Using both FITC-I permeability assay and TEM observation, we demonstrated that 2-BP administration rescued PA-induced BTB damage *in vivo* (Fig. 2D and E). Thus, PA-induced over-palmitoylation most likely leads to the disruption of Sertoli cell barriers, which further results in spermatogenesis dysfunction.

A

- HA   + HA   kDa

HRP-Strep

β-Actin

Control   PA   2-BP + PA
Control   PA   2-BP + PA

B

kDa

HRP-Strep

β-Actin

PA   - + - +   - + - +   - + - +
HA   - - + +   - - + +   - - + +
Sertoli   Leydig   Germ

C

CHOP
GRP78
ATF4
ATF6
β-Actin

PA   -   +   +
2-BP   -   -   +

D

Control

PA

2-BP + PA

E

F

G

ZO-1
OCLN
CLDN11
CLDN5
β-Actin

PA   -   +   +
2-BP   -   -   +

(caption on next page)

Fig. 4. Inhibition of protein palmitoylation ameliorates PA induced Sertoli cell dysfunction. (A) Analysis of the palmitoylation levels of proteins extracted from the testes of mice administered or not administered the PA injection, with or without gavage of 2-BP (n = 6 for Control, n = 7 for PA and 2-BP + PA). **(B)** Analysis of the palmitoylation levels of proteins extracted from primary Sertoli cells, Leydig cells and germ cells, which were treated with or without 0.4 mM PA (n = 3). **(C)** Inhibition of palmitoylation by 2-BP suppressed PA-induced ER stress in Sertoli cells. Translational expression levels of ER stress-related genes were analyzed using Western blotting (n = 3). **(D)** ROS detection using DCFH-DA staining. The fluorescence densities were calculated using ImageJ (n = 3). Scale bar: 50 μm. **(E)** TER detection of primary Sertoli cell barriers. The cells were incubated with PA (PA), with PA combined with 2-BP (2-BP + PA), or with the vehicle (Control) for 3 days after barriers were formed on day 4 (n = 5). **(F)** FITC-dextran permeability assessment of primary Sertoli cell barriers. The cells were treated PA (PA), with PA combined with 2-BP (2-BP + PA), or with the vehicle (Control) for 24 h after cell barriers were formed (n = 5). **(G)**Tight junction protein levels were examined by western blotting in TM4 Sertoli cells (n = 3). The relative intensities of bands in western blotting results were quantified by ImageJ and normalized to β-actin levels. Data are presented as mean ± SD. n. s., no significant difference vs. Control group. *P < 0.05, **P < 0.01 and ***P < 0.001 vs. Control group. #P < 0.05, ##P < 0.01 and ###P < 0.001 vs. PA group.
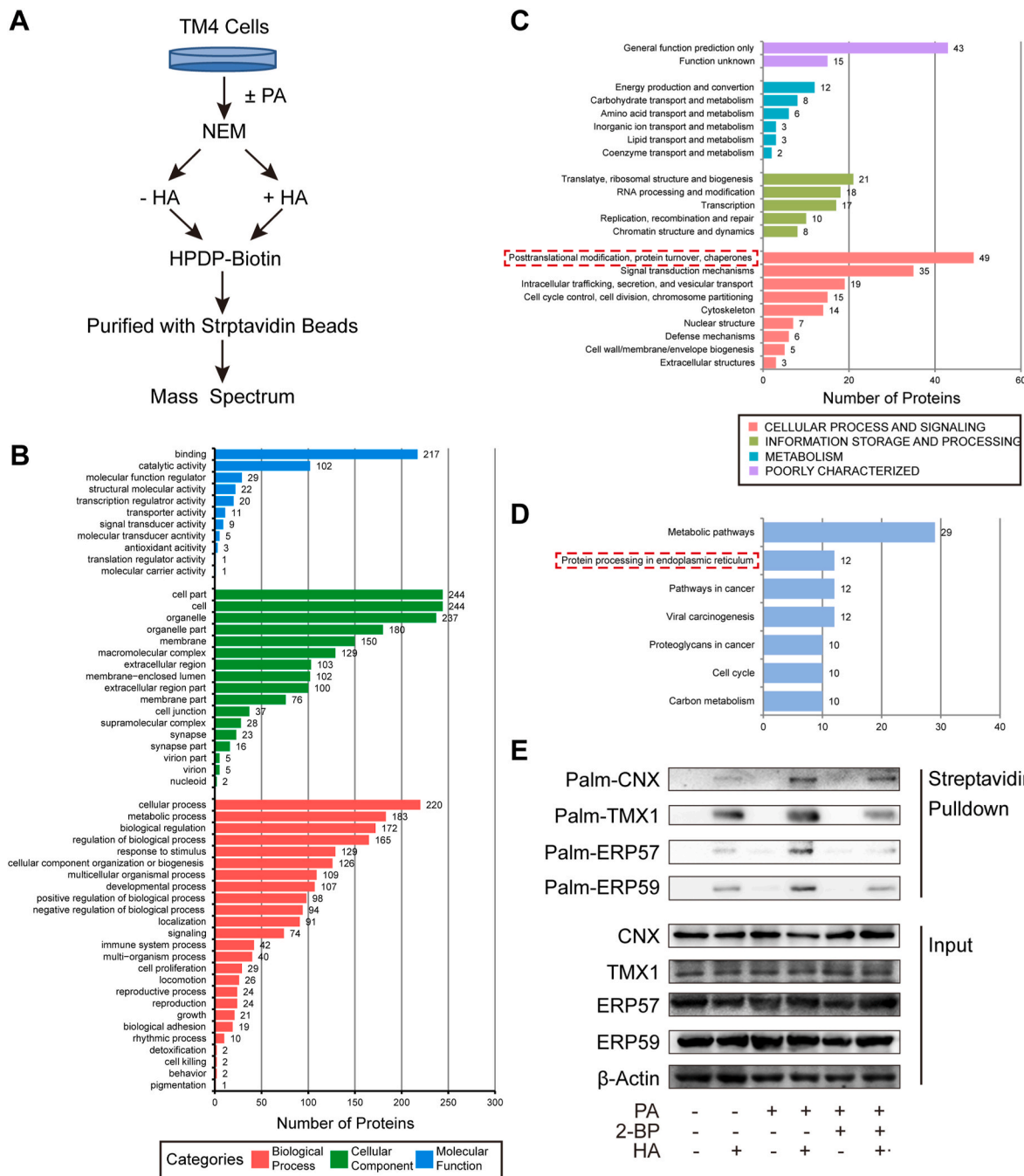

Fig. 5. Identification of palmitoylated proteins regulated by PA. (A) The flowchart illustrating the mass spectrum analysis of palmitoylated proteins regulated by PA. **(B–D)** GO (B), COG (C) and KEGG pathway (D) analysis of proteins whose palmitoylation levels were up-regulated after PA treatment in TM4 cells. **(E)** Detection of palmitoylation levels of ER proteins predicted to be regulated by PA. TM4 cells were treated by PA, with or without 2-BP pretreatment.

2.7. Inhibition of palmitoylation also alleviates PA-induced Sertoli cell apoptosis

Now we have found that PA-induced over-palmitoylation could disrupt Sertoli cell barriers, and a decrease of the expression of tight junction proteins is involved in this process. However, a loss of Sertoli cell viability may also lead to barrier disruption. We previously found that PA induces Sertoli cell apoptosis [9]. Also, after CHOP activation, apoptosis is reported to be a key mode of cell death [25]. Therefore, we analyzed apoptosis after PA and 2-BP treatment. Our results indicated that PA-induced apoptosis of Sertoli cells could be alleviated by 2-BP (Fig. S6A). After inhibiting apoptosis using apoptosis inhibitor

Z-VAD-FMK, PA-induced Sertoli cell barrier disruption was alleviated. However, in the presence of Z-VAD-FMK, 2-BP still showed an ameliorating effect of cell barrier disruption compared to the group treated with only PA and Z-VAD-FMK (Figs. S6D–E). Therefore, apoptosis is involved in Sertoli cell barrier disruption caused by PA through inducing over-palmitoylation, but other mechanisms should not be excluded, and the improvement of the expression of tight junction proteins is a considerable mechanism.
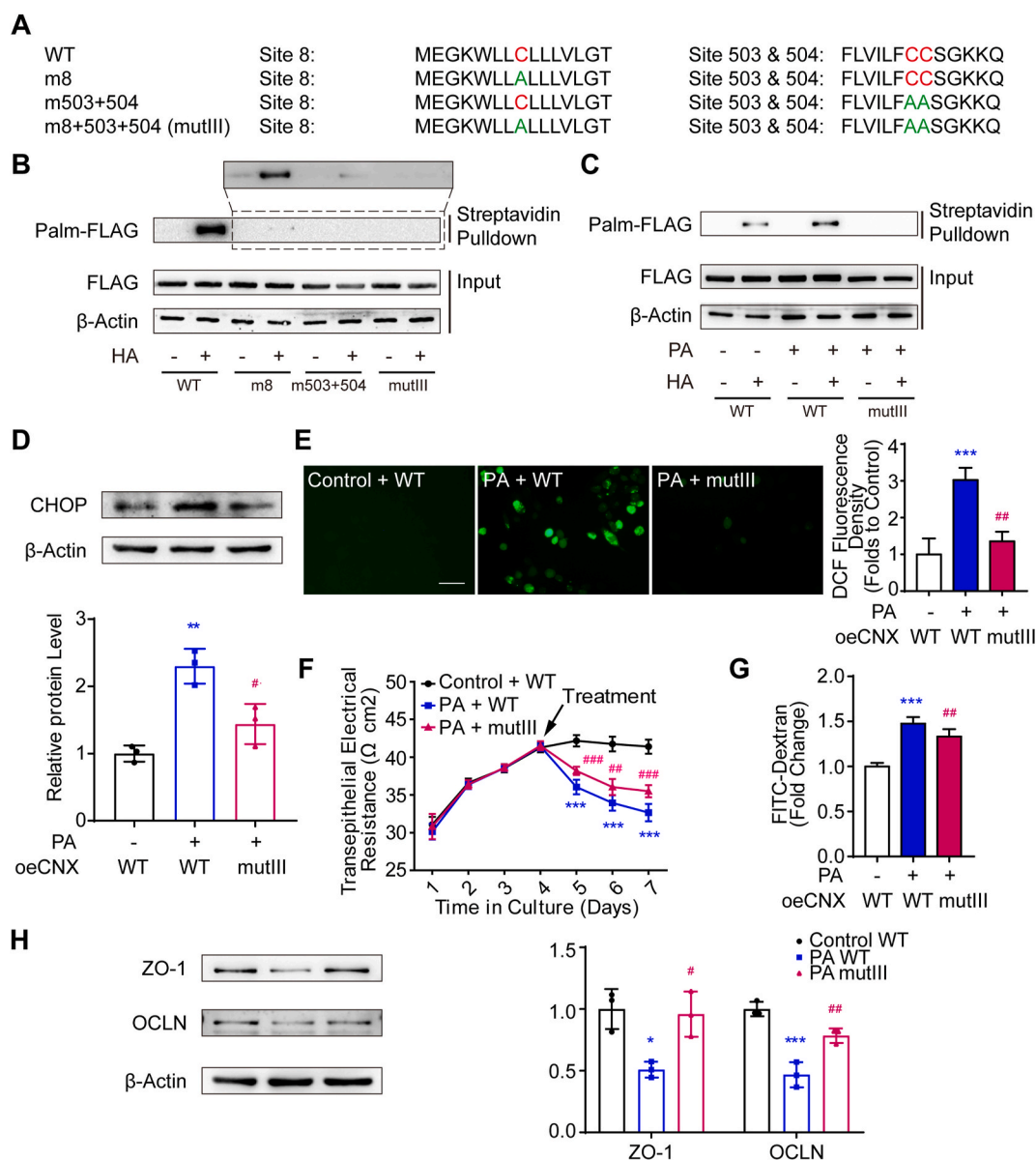
Fig. 6. The palmitoylation of calnexin is involved in PA-induced cell barrier disruption in Sertoli cells. (A) Sequences of wild type (WT) and mutated calnexin fragments. The predicted palmitoylation sites are marked with red color, and the mutated sites are marked with green color. **(B)** The palmitoylation of exogenous calnexin was validated, and sites 8, 503 and 504 were found to be its palmitoylation target sites. **(C)** The palmitoylation of exogenous calnexin was up-regulated by PA, while the mutation of all three target sites diminished palmitoylation. **(D)** Western blotting results indicated that mutation of all three palmitoylation target sites in calnexin alleviated PA-induced upregulation of CHOP (n = 3). **(E)** Mutation of all three palmitoylation target sites in calnexin alleviated PA-induced ROS production in Sertoli cells. ROS production was detected using DCFH-DA staining. The fluorescence densities were calculated using ImageJ (n = 3). Scale bar: 50 μm. **(F, G)** Mutation of all three palmitoylation target sites in calnexin ameliorated PA-damaged Sertoli cell barrier. TER detection (F, n = 7) and FITC-dextran permeability assays (G, n = 5) were used to detect the cell barrier integrity. **(H)** Tight junction protein levels were examined by western blotting. The relative intensities of bands were quantified by ImageJ and normalized to β-actin levels (n = 3). Data are presented as mean ± SD. *$P < 0.05$, **$P < 0.01$ and ***$P < 0.001$ vs. Control group; #$P < 0.05$ and ##$P < 0.01$ vs. PA group. (For interpretation of the references to color in this figure legend, the reader is referred to the Web version of this article.)

2.8. Variation of ER protein palmitoylation after PA stimulation and 2-BP treatment

Now we know that protein palmitoylation plays an important role in PA-induced Sertoli cell barrier disruption. However, the palmitoylated proteins involved in this process remained unknown. Thus, we purified palmitoylated proteins in Sertoli cells treated with or without PA using acyl-biotin exchange (ABE) assay, and compared protein palmitoylation in control and PA-treated Sertoli cells using mass spectrometry (Fig. 5A). The proteins showing higher palmitoylation levels in PA-treated cells were screened out for Gene Ontology (GO), Cluster of Orthologous Groups of proteins (COG) and KEGG Pathway annotation (Fig. 5B–D). Both COG and KEGG Pathway annotation showed an enrichment of proteins relating to ER functions, i.e. "Posttranslational modification, protein turnover, chaperones" in COG, and "Protein processing in endoplasmic reticulum" in KEGG Pathway. Among the 12 palmitoylated proteins involved in the pathway "Protein processing in endoplasmic reticulum", 7 proteins show ER location, in which 4 proteins directly function in the regulation of protein folding, including CNX, thioredoxin related transmembrane protein 1 (TMX1), protein disulfide-isomerase A3 precursor (PDIA3/ERP57) and prolyl 4-hydroxylase, beta polypeptide (P4hb/PDIA1/ERP59) (Table S3).

According to our previous results, PA enters ER after being incorporated by Sertoli cells. Also, dysfunction of protein folding is upstream of ER stress. Thus, we focused on ER proteins regulating protein folding, and the up-regulation of palmitoylation levels of these 4 proteins by PA was validated. Moreover, the palmitoylation levels of these proteins were also decreased by palmitoylation inhibitor 2-BP (Fig. 5E).

2.9. Palmitoylation of CNX plays a critical role in PA-induced Sertoli cell barrier disruption

According to the mass spectrometry results, among the 4 proteins functioning in the regulation of protein folding, CNX showed the most dramatic up-regulation of palmitoylation level after PA stimulation (Ratio = 7.43, Table S3). Thus we furtherly studied whether CNX palmitoylation is involved in PA-induced Sertoli cell barrier disruption. Firstly, we predicted palmitoylation sites in CNX using CSS-PALM (http://csspalm.biocuckoo.org/) and NBA-PALM (http://nbapalm.biocuckoo.org/), and identified Cys-8, Cys-503 and Cys-504 as the potential palmitoylation sites (Fig. 6A). Among these sites, Cys-503 and Cys-504 have been demonstrated to be palmitoylated before [26]. Cys-8 is a newly identified palmitoylation site of CNX. As shown in Fig. 6B, mutation of Cys-8 into alanine significantly decreased palmitoylation of CNX. Moreover, while CNX with mutations of both Cys-503 and Cys-504 still showed a weak palmitoylation, mutations of all three sites (mIII) diminished CNX palmitoylation completely (Fig. 6B). In PA-treated Sertoli cells, mIII also diminished CNX palmitoylation (Fig. 6C). When Sertoli cells were transfected with CNX containing mIII, ER stress and ROS production induced by PA was alleviated (Fig. 6D and E), and the Sertoli cell barrier was recovered (Fig. 6F–H). These results demonstrate that CNX palmitoylation play a considerable role in the regulation of ER stress activation and cell barrier integrity damage.

2.10. Disruption of calcium balance is involved in PA-induced Sertoli cell barrier disruption

The palmitoylation of CNX has been reported to modulate its interaction with sarcoendoplasmic reticulum (SR) calcium transport ATPase (SERCA) 2b, and this interaction regulates ER-mitochondria calcium crosstalk [27]. Thus we analyzed calcium balance in Sertoli cells by using cytosolic Ca^{2+} indicator Fluo-3 and mitochondrial Ca^{2+} indicator Rhod-2 for staining. According to the results, PA increased both cytosolic and mitochondrial Ca^{2+} concentrations, while 2-BP down-regulated both Ca^{2+} concentrations (Figs. S7A and S7B). As the imbalance of calcium between ER and mitochondria may impair their interaction and cause mitochondrion dysfunction, we analyzed mitochondrial ROS by using MitoSOX to indicate mitochondrial superoxide. The results showed that PA increased mitochondrial ROS, which was decreased by 2-BP (Fig. S7C). These results indicate that a disruption of calcium balance happened in Sertoli cells after PA-induced over-palmitoylation.

Moreover, mutation of CNX palmitoylation sites alleviated both Ca^{2+} concentrations (Figs. S8A and S8B). Therefore, we used a SERCA pump inhibitor thapsigargin to treat Sertoli cells. The results indicated that inhibition of SERCA rescued both Sertoli cell survival and cell barrier integrity (Figs. S8C–F). So we concluded that calcium balance disruption, which is regulated by CNX palmitoylation, was involved in tight junction disruption induced by PA.

2.11. ω-3 PUFAs ameliorates PA-induced spermatogenesis dysfunction, BTB disruption and excessive palmitoylation in vivo

According to the serum fatty acid composition analyzed in this study, SFA/USFA ratio was higher in men with NOA or EO (Fig. 1D). USFAs are essential for spermatogenesis, and supplementation of USFAs has already been proved to improve male fertility [28]. ω-3 PUFAs are a representative class of USFAs, which has been discovered to alleviated a series of symptoms caused by dyslipidemia [29]. Therefore, we explored whether ω-3 PUFAs have an ameliorating effect on PA-induced spermatogenesis dysfunction, and whether palmitoylation regulation is involved in this process.

We gavaged mice with ω-3 PUFAs simultaneously to PA administration, and found that ω-3 PUFAs significantly recovered sperm concentration and sperm motility (Fig. 7A and B). The effects of ω-3 PUFAs on sex hormones are similar to that of 2-BP, that is to say, ω-3 PUFAs also did not recover the level of FSH, LH or INHB (Fig. 7C, S9F and S9G). On the other hand, ω-3 PUFAs recovered PA-induced BTB damage in mouse testes (Fig. 7D and E), indicating a rescuing effect of ω-3 PUFAs on Sertoli cell barrier function. We furtherly detected protein palmitoylation in testes, and found that ω-3 PUFAs decreased palmitoylation obviously (Fig. 7F), suggesting a possible involvement of palmitoylation regulation by ω-3 PUFAs in this process.

2.12. ω-3 PUFAs alleviate PA-induced Sertoli cell damage and excessive palmitoylation in vitro

The ameliorating effect of ω-3 PUFAs on PA-induced ER stress in Sertoli cells was validated *in vitro*. A pre-treatment of Sertoli cells with ω-3 PUFAs (25, 50, 100 and 200 μM) substantially alleviated PA-induced over-expression of ER stress markers, and the concentration of 200 μM showed the most dramatic rescuing effect, which was validated by quantitative RT-PCR analysis (Fig. S10A). Thus 200 μM was selected for further analysis of ω-3 PUFA effects. Protective effect of ω-3 PUFAs against PA-induced ER stress was also proved by decreased protein expression levels of ER stress markers (Fig. 8A) and by reduced ROS generation (Fig. 8B).

On the other hand, the effect of ω-3 PUFAs on Sertoli cell barrier was also investigated. Both TER and FITC-dextran permeability assays showed a protection by ω-3 PUFAs against PA-damaged barrier disruption (Figs. 8C, 8D, S10B and S10C). The expression levels of tight junction proteins were also recovered by ω-3 PUFA treatment (Fig. 8E). Therefore, the protective role of ω-3 PUFAs on Sertoli cell barrier maintaining was validated.

Protein palmitoylation analysis revealed that ω-3 PUFAs, like 2-BP, significantly decreased palmitoylation level in Sertoli cells *in vitro*, which was increased by PA (Fig. 8F). Combining with the palmitoylation alleviating effects of ω-3 PUFAs in testes *in vivo* (Fig. 7F), we can infer that ω-3 PUFAs modulate protein palmitoylation in Sertoli cells. Moreover, the palmitoylation level of the ER protein CNX, which has been demonstrated to participate in the regulation of ER stress activation and cell barrier integrity damage in Sertoli cells, was alleviated by ω-3
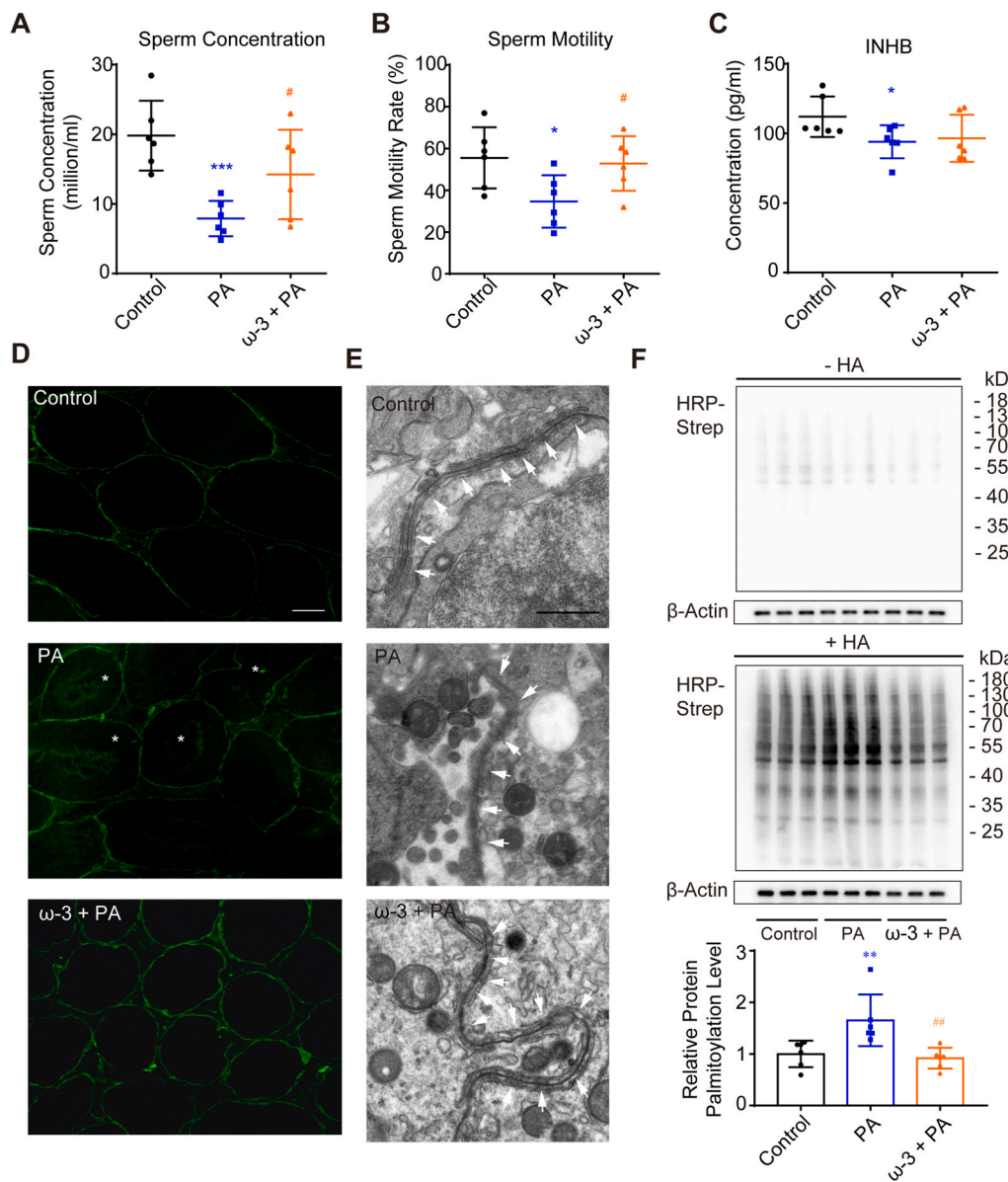
Fig. 7. ω-3 PUFAs rescues PA-induced spermatogenesis dysfunction in mice. Mice were injected intraperitoneally (i. p.) with BSA (Control group) or PA-BSA (PA group) (n = 6 per group) once daily for 30 days, with or without gavage of ω-3 PUFAs every two days. **(A, B)** Sperm concentrations (A) and sperm motilities (i.e. percentage of mobile sperms) (B) were assessed using a haemocytometer. **(C)** Concentrations of INHB in serums were analyzed by ELISA. Data are presented as mean ± SD. *$P < 0.05$ and ***$P < 0.001$ vs. Control group. #$P < 0.05$ vs. PA group. **(D)** Assessment of BTB integrity *in vivo* using FITC-I permeability assays. Asterisks (*) indicate leaked FITC-I in the lumen of seminiferous tubules. Scale bars: 100 μm. **(E)** The ultrastructure of tight junctions was observed using transmission electron microscopy. White arrows indicate the tight junctions. Scale bars: 1 μm. **(F)** Analysis of the palmitoylation levels of proteins extracted from the testes of mice administered or not administered the PA injection, with or without gavage of ω-3 PUFAs. The relative intensities of bands were quantified by ImageJ and normalized to β-actin levels (n = 6). Data are presented as mean ± SD. **$P < 0.01$ vs. Control group; ##$P < 0.01$ vs. PA group.

PUFAs (Fig. 8G). The other ER proteins that were previously validated to be over-palmitoylated by PA, were also found to be modulated by ω-3 PUFAs on their palmitoylation levels (Fig. S10D). These results indicate that ω-3 PUFAs may ameliorate PA-induced cell damage by adjusting the palmitoylation levels of CNX, and possibly some other ER proteins.

Besides ω-3, ω-6 is also a major type of PUFAs. To investigate whether the palmitoylation regulating effect is specific to ω-3 PUFAs, we used a representative ω-6 PUFA, arachidonic acid (AA), to treat Sertoli cells. According to the results, AA rescued both PA-induced decrease of Sertoli cell survival and disruption of cell barrier integrity (Figs. S10E and S10F). Meanwhile, AA significantly alleviated PA-induced over-palmitoylation in Sertoli cells (Fig. S10G). Therefore, it can be inferred that PUFAs may participate in modulating palmitoylation levels and thus improve Sertoli cell functions in dyslipidemia conditions.

3. Discussion

Current information about male infertility causes includes genetic factors, environmental factors, age, life-style, and so on. Metabolic disorder is also an important factor leading to male infertility in the modern world. Although the prevalence of hyperlipidemia has been reported to

be significantly higher in infertile men [30], the critical type of lipid disturbing male fertility remains unclear. According to our clinical data, the levels of PA increased in the serum of patients with severe dyszoospermia (NOA and EO) (Fig. 1), providing a direct evidence supporting that excess PA is detrimental to spermatogenesis. As elevated dietary, seminal plasma and spermatozoal PA levels have been proved to negatively associate with male fertility [31–34], our results connected these points with the circulating PA. Also, our data focused on the relationship between PA and dysfunction in spermatogenesis, which is the first critical step before sperm maturation, and is reflected mostly by sperm concentration. An elevated serum PA level accompanied with frustrated spermatogenesis leads us to explore the mechanism underlying this correlation. According to a significant decrease of INHB in the serum of patients with severe dyszoospermia (Fig. 1G), a correlation between elevated PA levels and Sertoli cell dysfunction was speculated.

One of the most important functions of Sertoli cells is the formation of the BTB. We previously identified abnormal ZO-1 expression and distribution in the testes of patients with nonobstructive azoospermia [35], which emphasized the indispensable role of BTB on spermatogenesis. We previously showed that PA decreases Sertoli cell survival [9, 10]. In the present study, we demonstrated that PA is a risk factor for
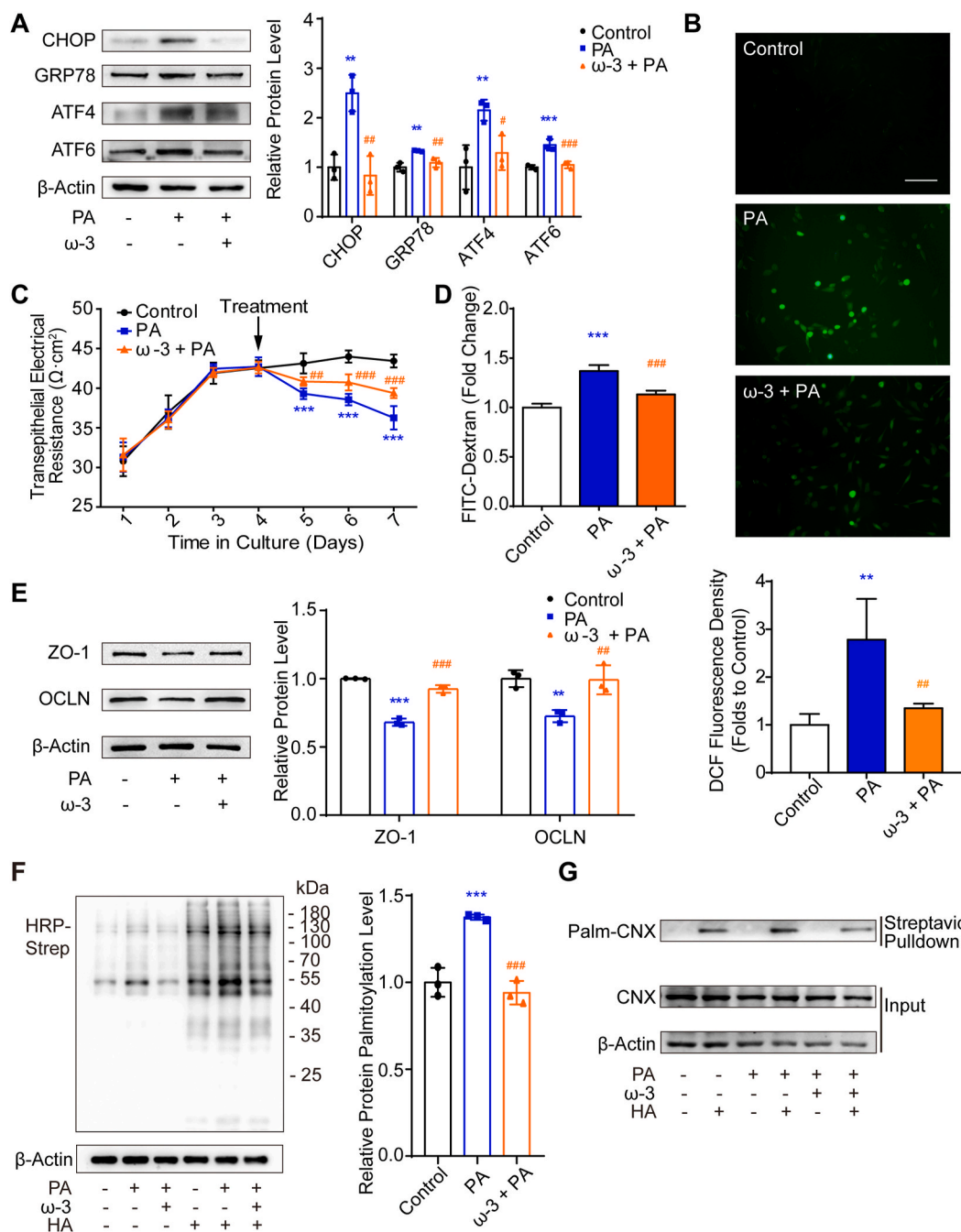
Fig. 8. ω-3 PUFAs ameliorate PA-induced Sertoli cell dysfunction and protein over-palmitoylation. (A) ω-3 PUFAs suppressed PA-induced ER stress in Sertoli cells. TM4 cells were treated by PA, with or without a pretreatment of ω-3 PUFAs. Translational expression levels of ER stress-related genes were analyzed using Western blotting. The relative intensities of bands were quantified by ImageJ and normalized to β-actin level (n = 3). **(B)** ROS detection using DCFH-DA staining. The fluorescence densities were calculated using ImageJ (n = 3). Scale bar: 50 μm. **(C, D)** Assessment of cell barrier integrity *in vitro*. After cell barrier formation, cells were incubated with PA (PA), with PA combined with ω-3 (ω-3 + PA), or with the vehicle (Control). TER detection (C, n = 8) and FITC-dextran permeability assays (D, n = 5) were used to analyze the integrity of primary Sertoli cell barriers. **(E)** Tight junction protein levels in TM4 Sertoli cells were examined by western blotting. The relative intensities of bands were quantified by ImageJ and normalized to β-actin levels (n = 3). **(F)** Analysis of the palmitoylation levels of proteins extracted from PA-treated TM4 cells with or without a pretreatment with ω-3 PUFAs. The relative intensities of bands were quantified by ImageJ and normalized to β-actin levels (n = 3). **(G)** Detection of palmitoylation levels of CNX in TM4 cells treated by PA, with or without pretreatment of ω-3 PUFAs. Data are presented as mean ± SD. **P < 0.01 and ***P < 0.001 vs. Control group. #*P* < 0.05, ##*P* < 0.01 and ###*P* < 0.001 vs. PA group.

Sertoli cell barrier dysfunction (Figs. 2 and 3 and S2). A recently published study demonstrated that intraperitoneal injected PA shows lipotoxicity in mouse testes, and may affect germ cells [36]. However, the invasion of PA into the seminiferous tubules has not been clarified before, and so the direct effect of PA on germ cells needs further confirmation. Our results demonstrated that PA enters Sertoli cells and

disrupts BTB (Figs. 2 and 3 and S2). Thus, PA from the blood may directly affect Sertoli cells, and then enter seminiferous tubules through either Sertoli cells or disrupted BTB. Such a finding could expand our knowledge on the mechanism underlying PA induced testis toxicity.

Our findings supported the involvement of ER stress signaling in PA-induced Sertoli cell barrier disruption (Figs. 3, S2, S3 and S4). The

damage of ER structure induced by PA was detected not only by electron microscopy observation, but also by a dynamic observation using ER tracker staining. A sequential observation of ER after 30 min of PA treatment indicated that PA plays a role shortly after its addition (Fig. 3F, Videos S1 and S2). A long-term treatment of PA for 24 h exacerbated ER damage (Fig. 3G). Therefore, the injury to ER by PA is rapid and persistent, which leads to ER stress and Sertoli cell barrier destruction. There is ample evidence that amelioration of ER stress is a promising strategy to treat metabolic diseases, including dyslipidemia [37]. Reduction of ER stress could also prevent the disruption of tight junction barriers [14], which was demonstrated in Sertoli cells by our results (Figs. S3 and S4). Thus alleviation of ER stress is a potential means to improve Sertoli cell barriers disrupted by PA and in dyslipidemia.

In this study, we found activation of the PERK and ATF6 branches of the UPR. And we furtherly validated that inhibition of PERK branch, but not ATF6 branch, of the UPR shows an alleviating effect on PA-induced barrier disruption, indicating an involvement of PERK pathway in regulating Sertoli cell barrier integrity. As PERK pathway has been found to be involved in epithelial barrier injury [38], this result provides a new evidence for targeting PERK pathway in restoring the integrity of cell barriers. Interestingly, PERK pathway has been proposed to function as a calcium sensor in ER, and play a role in cellular response to calcium concentration [39]. Consistent with this, we found that calcium balance is disrupted in PA-induced Sertoli cell barrier destruction, which is recovered after 2-BP treatment (Fig. S7). Therefore, PERK pathway is critical in PA-induced Sertoli cell dysfunction, and a causal relationship between calcium balance disruption and PERK pathway may exist in this process.

Protein palmitoylation participates in the activation of ER stress signaling in some cell types [40,41]. According to our results, we found that inhibition of palmitoylation ameliorated PA-induced BTB disruption, as well as ER stress and barrier destruction in Sertoli cells, indicating that palmitoylation is involved in this process (Figs. 2 and 4 and S5). Therefore, a critical role of protein palmitoylation in the regulation of Sertoli cell functions is speculated. The discovery that disruption of Sertoli cell barriers triggered by PA is mediated by abnormal palmitoylation introduces over-palmitoylation into male infertility. Also, as shown in Fig. 1E, stearic acid (SA; C18:0) is the second abundant SFA in serum, and SA has also been reported to induce cell dysfunction [42], as well as has a higher concentration in infertile men [43]. SA, although is not the most common substrate for palmitoylation, could also be transferred to protein cysteines by some DHHC S-acyltransferases [44]. Therefore, SA may also participate in the harmful effects on spermatogenesis microenvironment, and palmitoylation may also be a critical mechanism involved. These suggest that modulation of protein palmitoylation is a candidate option for the treatment of dyszoospermia accompanied with dyslipidemia.

To clarify the mechanism underlying PA-induced Sertoli cell barrier destruction due to over-palmitoylation, we analyzed both apoptosis and tight junction protein expression. When both apoptosis inhibitor Z-VAD-FMK and 2-BP were added for Sertoli cell treatment, the rescuing effect on PA-induced barrier disruption is obviously more remarkable than Z-VAD-FMK was added only (Figs. S6D and S6E). So we can conclude that although apoptosis is involved in this process, there may be other mechanisms. As we observed improvement of the expression of tight junction proteins (Fig. 4G), and CHOP silencing has been found to improve the expression of tight junction proteins by others [45], it can be inferred that the regulation of tight junction protein expression is also a critical mechanism.

In consistent with the fact that PA enters ER in Sertoli cells as we confirmed, proteins regulating ER functions were found to be a major class of palmitoylated proteins modulated by PA (Fig. 5). In fact, protein folding is a most important function of ER, and ER stress is induced by abnormal accumulation of unfolded proteins in ER, so the proper regulation of protein folding is vital for cell status. We identified 4

proteins directly functioning in the regulation of protein folding, whose palmitoylation levels were elevated by PA and decreased by 2-BP. Among them, CNX showed the most dramatic up-regulation of palmitoylation level after PA stimulation. CNX is a key chaperone participating in protein folding in ER, and its palmitoylation on Cys-503 and Cys-504 has been reported before [17,26]. Our study identified a third palmitoylation site, Cys-8 (Fig. 6). As CNX has been reported to regulate PERK and ATF6 pathways, its abnormal palmitoylation induced by PA may disrupt ER status [46,47]. Our further analysis validated that palmitoylation of CNX modulates the ER status, and also cell barrier functions in Sertoli cells (Fig. 6). Such a result is consistent with a previously reported work, in which CNX was found to function in blood-brain barrier integrity against T-cell penetration [48]. Moreover, as CNX regulates calcium crosstalk between ER and mitochondria by interacting with SERCA, we validated that calcium balance is regulated by CNX palmitoylation, and that SERCA is involved in cell barrier damage by PA (Fig. S8). These results proved that regulation of calcium balance by CNX palmitoylation may play a role in cell barrier integrity regulation. Therefore, our study discovered the involvement of CNX in BTB integrity maintenance, and proposed that the palmitoylation of CNX may regulate this integrity by influencing ER status.

Our results prompted that over-palmitoylation of proteins in Sertoli cells leads to BTB disruption and spermatogenesis dysfunction. Therefore, modulation of palmitoylation may help improving spermatogenesis. Palmitoylation is a reversible lipid modification regulated by Asp-His-His-Cys (DHHC) S-acyltransferases which promotes palmitoylation, and certain serine hydrolases functioning as S-deacylases to induce depalmitoylation [44]. In our study, PA is the substrate of palmitoylation, so excess PA can induce over-palmitoylation. To decrease palmitoylation, there are some reported palmitoylation inhibitors, such as 2-BP and cerulenin, which suppress DHHC S-acyltransferases [49]. However, 2-BP, which is used in our study, as well as cerulenin, have not been proved to be clinically safe medicines. We furtherly tried to explore an eligible medicine to protect BTB against PA-induced damage. As a representative class of USFA, ω-3 PUFAs have attached attention due to the therapeutic effects and a wide range of food sources. In our formerly published paper, we already demonstrated a protective role of ω-3 PUFAs on PA-induced Sertoli cell toxicity [9]. In this study, we further confirmed the effects of ω-3 PUFAs on PA-induced ER stress and cell barrier damage in Sertoli cells both *in vivo* and *in vitro* (Figs. 7 and 8 and S10). Interestingly, a down-regulation of protein palmitoylation induced by PA was observed after ω-3 PUFA treatment (Figs. 7 and 8 and S10). The palmitoylation of CNX was also alleviated by ω-3 PUFAs (Fig. 8G). We also discovered palmitoylation alleviating effects of ω-6 PUFAs, accompanied with cell barrier recovering effects on PA-induced Sertoli cell barrier damage (Figs. S10E–G). The suppression of palmitoylation by ω-3 and ω-6 PUFAs is in accordance with a previously published study, in which a similar phenomenon was found in T cells [50]. These results indicate a possible relationship between palmitoylation regulation and the protective role of PUFAs. It has been reported that although PA is the most commonly attached lipid in S-palmitoylation, other fatty acids including USFAs can also modify lipoproteins, so S-palmitoylation is also called S-acylation [51,52]. But the mechanism underlying the regulation by PUFAs on palmitoylation remains unclear, and this question should be a key point in the further research. Nevertheless, the protective role of PUFAs on BTB is confirmed, and a diet with adequate PUFAs is recommended for male fertility protection. Also, other palmitoylation inhibitors still needs to be discovered for male fertility improvement.

In conclusion, our study demonstrated the involvement of PA and palmitoylation in the pathogenesis of spermatogenesis dysfunction. Our clinical results revealed that the PA levels are significantly higher in patients with severe dyszoospermia, i.e. NOA and EO. The studies *in vivo* and *in vitro* indicated that PA disrupts BTB by damaging tight junctions between Sertoli cells, and ER stress plays a critical role in this process. Aberrant palmitoylation is an important cause of ER stress and

subsequent cell barrier damage after PA treatment. A screen for palmitoylated proteins involved in PA-induced Sertoli cell dysfunction was executed, and CNX was found to play a critical role in regulating ER status and cell barrier in Sertoli cells by its palmitoylation level variation. We also found that ω-3 PUFAs, a representative class of USFAs, showed protective roles on PA-induced BTB disruption, and an alleviation of excessive palmitoylation. Collectively, these results indicate that palmitoylation is a crucial regulator of Sertoli cell function (Fig. 9), which may provide novel targets for treating dyszoospermia accompanied by Sertoli cell dysfunction and disordered lipid metabolism.
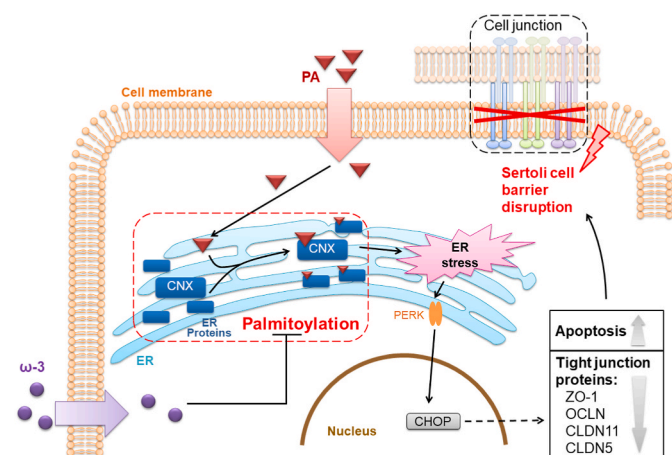
4. Materials and methods

4.1. Collection of human serum samples

Serum samples were collected between 8:00 and 11:00 a.m. from 25 patients with NOA (n = 22) or EO (n = 3) and 25 healthy individuals (controls) who were undergoing routine semen analysis at our clinical laboratory (Table S1) between September 2017 and January 2020. All the individuals were aged from 20 to 43 years old. The blood samples were centrifuged at room temperature for 10 min at $1800 \times g$, and then serum samples were taken and stored at -70 °C. Sperm quality was analyzed using a WLJY-9000 computer-assisted system (WLJY-9000, WeiLi Co., Ltd, Beijing, China). Normal sperm criteria was defined as sperm concentration $>15 \times 10^6$/mL, progressive motility $>32\%$, total motility $>40\%$ and normal sperm morphology rate $>4\%$. NOA was defined as no sperm observed in either semen analysis or testicular biopsy, excluding chromosomal karyotype abnormalities and AZF region deletion. EO was defined as sperm concentration $<1 \times 10^6$/mL. The seminal fluid samples of all the three patients with EO were centrifuged, and 50 μl was taken out for each semen smear. Only 3 to 10 progressive sperms were observed in each sample, indicating that all these EO sperm samples also show extremely low progressive motility. All clinical samples were collected under informed consent and approved by the Research Ethics Committee of Jinling Hospital.

4.2. Serum inhibin B analysis

Serum inhibin B levels were measured using an iFlash Chemiluminescence Immunoassay Analyzer (YHLO Biotech, Shenzhen, China).

4.3. Serum fatty acid analysis

Serum free fatty acid levels were analyzed by GC/MS. In brief, the samples were thawed on ice and chloroform methanol solution was added. After ultrasonication, the supernatant was taken. Then 1% sulfuric acid-methanol solution was added and the mixtures were incubated at 80 °C for 30 min for free fatty acid methyl esterification. Thereafter, the methylated fatty acids were extracted by n-hexane and washed by water. The levels of methylated fatty acids were determined by GC/MS using Agilent 7890A/5975C gas chromatography-mass spectrometer with an Agilent DB-WAX capillary column (30 m×0.25 mm ID × 0.25 μm) (Agilent Technologies, CA, USA). In this analysis, 39 free fatty acids of medium and long-chain length (i.e., C6–C24) were quantified. The analysis was performed by Shanghai Applied Protein Technology Inc.

4.4. Animal and treatment

Four-week-old male ICR mice and eight-week-old male C57BL/6 mice (Beijing Vital River Lab Animal Technology Co., Ltd., Beijing, China) were housed at 20–26 °C under a 12/12 h light/dark cycle. Experimental procedures involving animals were conducted according to the NIH Guide for the Care and Use of Laboratory Animals and were approved by the Ethics Committee of the Nanjing Jinling Hospital. The ICR mice were intraperitoneally injected with 200 mg/kg body weight PA (Sigma-Aldrich, St. Louis, MO, USA) (conjugated with BSA, PA group) or the same volume of BSA (Yeasen, Shanghai, China) (Control group) once daily for 30 d [36,53]. In treatment groups, the mice were gavaged 40 mg/kg 2-BP (2-BP + PA group) or 2 g/kg ω-3 PUFAs (derived from fish oil, containing >90% ω-3 ethyl ester, and included at least 40% DHA and 32% EPA) (OMEGA 3 TREASURE, Shanghai, China) (ω-3 +PA group) every two days, simultaneous with PA injection [54,55].

4.5. Measurement of sperm concentrations and motilities in mice

Sperms from one of the cauda epididymis were released into 0.4 mL HTF medium and incubated for 5 min at 37 °C, and then sperm concentrations and motilities were determined using a haemocytometer (Qiujing, Shanghai, China) under a light microscope (Olympus, Tokyo, Japan).

4.6. Analysis of reproductive hormone levels in mouse serum

Blood samples from mice were centrifuged at 4 °C for 10 min at 4000 rpm, and the serum was collected for hormone detection. FSH, LH, INHB and T levels in serum samples were analyzed by ELISA kits (Cloud-Clone Corp, Wuhan, China) according to the manufacturer's instructions.

4.7. Assessment of BTB integrity in vivo by FITC-I permeability assay

Freshly diluted FITC-I (Sigma-Aldrich; 200 μL) in PBS (5 mg/mL) was injected into the caudal vein of each mouse. The mice were sacrificed by neck breaking 2 h later, and then, their testes were dissected and flash frozen in liquid nitrogen for BTB integrity assays. The testes were embedded in Optimal cutting temperature compound and sectioned to 8-μm thickness using a cryostat microtome. Images were acquired on a fluorescence microscope (IX73; Olympus Corporation, Tokyo, Japan) equipped with a 10 × objective.

4.8. Electron microscopy

Small pieces of testicular tissues or Sertoli cells were collected and fixed with 0.1 M phosphate buffer containing 2.5% glutaraldehyde (Servicebio Wuhan, China), and then sequentially stained with 1% osmium tetroxide, 2% uranyl acetate solution and lead citrate (all from Servicebio). Embedded cells were sectioned and visualized using a

Fig. 9. Mechanism of Sertoli cell barrier disruption induced by PA. PA enters Sertoli cells, penetrates ER, and palmitoylates ER proteins. Palmitoylated CNX and other ER proteins activate ER stress, especially PERK pathway, promote cell apoptosis and down-regulate tight junction proteins by inducing CHOP expression, and finally disrupt Sertoli cell barrier. On the other hand, ω-3 PUFAs alleviates the palmitoylation of ER proteins and Sertoli cell dysfunction induced by PA.

transmission electron microscopy (HITACHI, Tokyo, Japan).

4.9. Isolation and culture of primary mouse Sertoli cells, leydig cells and germ cells

Primary mouse Sertoli cells for cell barrier analysis were isolated from the testes of 20-day-old ICR mice (Beijing Vital River Laboratory Animal Technology Co., Ltd). The isolation was executed using a two-step enzyme digestion method as previously described [10]. Cells were cultured in Dulbecco's modified Eagle's medium/Ham's nutrient mixture F12 (DMEM/F12; Yuanye, Shanghai, China) supplemented with 10% fetal bovine serum (FBS; Gibco; Thermo Fisher Scientific, Inc., Waltham, MA, USA) at 37 °C under a 5% CO_2 atmosphere for two days. Then the cells were treated with 20 mM Tris (pH 7.4) for 3 min to remove germ cells, washed with PBS and cultured until use.

Primary cells for palmitoylation analysis were isolated from the testes of 8-week-old ICR mice. Primary Sertoli cells were isolated as described above. Primary Leydig cells were isolated using a density gradient centrifugation method according to a previously published method [56]. Primary germ cells were also isolated referring to a method previously reported [57]. Inbrief, decapsulated testes were minced by scalpels, and Sertoli cells and tissue fragments were removed by twice pelleting at $100 \times g$. Then the supernatant was filtered sequentially with 100-μm and 40-μm cell strainer (BD Falcon, BD Biosciences, Bedford, MA, USA), and germ cells were collected by centrifuging at $500 \times g$ for 10 min. In order to mimic the status *in vivo*, all the isolated primary cells were used for experiment immediately after attachment to dishes, and DMEM/F12 was used for cell incubation.

4.10. Culture of TM4 cell line

Mouse TM4 Sertoli cells (iCell Bioscience, Inc., Shanghai, China) were cultured in DMEM/F12 supplemented with 10% FBS at 37 °C under a 5% CO_2 atmosphere.

4.11. Cell treatment

PA at the dose of 0.4 mM was used to induced Sertoli cell damage. This dose is determined according to estimated concentration of PA in serum and the dose commonly applied in the studies of PA [58–63].

For rescuing experiments, 2-BP, GSK2606414 (Selleck, Shanghai, China), melatonin (Sigma-Aldrich), Z-VAD-FMK (Selleck), thapsigargin (Selleck), ω-3 PUFAs (OMEGA 3 TREASURE) or AA (Sigma-Aldrich) were used with a pretreatment for 2 h and then added for incubation as long as PA presents. The cell treatment doses of these reagents such as ω-3 PUFAs were determined referring to published studies [9,64–66].

4.12. Transepithelial resistance (TER) measurements

We measured TER to assess the integrity of functional cell barriers as follows: Sertoli (0.5×10^6 cells/cm^2) were seeded onto Millicell Hanging Cell Culture Inserts (PET 0.4 μm, Merck Millipore, Billerica, MA, USA) and cultured for 3 days to allow cell barrier formation. Then, the cells were treated, and the TER was monitored using a Millicell Electrical Resistance System (Merck Millipore). To analyze the effects of CHOP knockdown and mutated CNX over-expression on cell barrier formation, TM4 cells were transfected with indicated siRNAs or plasmids. Twenty-four hours after the transfection, cells were plated on Millicell Hanging Cell Culture Inserts and cultured. TER was monitored, and PA was added in the medium 3 days later when the cell barrier formed.

4.13. FITC-dextran permeability assessment

For FITC-dextran permeability assessment, TM4 cells and primary mouse Sertoli cells were also plated on Millicell Hanging Cell Culture Inserts. Once cell barriers formed, PA, 2-BP (Sigma-Aldrich), or TM (Abcam, Shanghai, China) were added to the medium. After 24 h, 1 mg/mL FITC-dextran (Sigma-Aldrich) diluted in 200 μL DMEM/F12 without phenol red (Yuanye) was added to the apical side, and 1.2 mL DMEM/F12 without phenol red was added in the basal chamber. After incubation for 4 h, a 200 μL sample was taken from the basal chamber, and the fluorescence emission at 520 nm was measured with excitation at 490 nm using a Synergy HTX Multi-Mode Microplate Reader (BioTek, Shanghai, China).

4.14. CCK-8 cell viability analysis

Cells were seeded in 96-well plates at a density of 5×10^3, and cultured overnight for attachment before treatment. After treatment, cell viabilities were analyzed using Cell Counting Kit-8 (Beyotime, Shanghai, China).

4.15. Cell apoptosis analysis

Cells were treated with PA and 2-BP for 24 h, and then the apoptotic rates were analyzed using Annexin V-FITC Apoptosis Detection Kit (Beyotime) and flow cytometry.

4.16. Western blotting

Cells were suspended in radioimmunoprecipitation assay protein extraction buffer for cell lysis and protein extraction [67]. Protein concentrations were determined using Pierce BCA protein analysis kit (Thermo Fisher Science, Inc.). For polyacrylamide gel electrophoresis, a total of 20 μg protein was loaded in each lane. After electrophoresis, proteins were transferred to PVDF membrane (Merck Millipore, Billerica, MA, USA), and exposed to primary and secondary antibodies successively. The main antibodies used include: rabbit polyclonal ZO-1 (1:1000; cat. no. 21773-1-AP; ProteinTech Group, Inc., Wuhan, China), rabbit polyclonal Occludin (1:1000; cat. no. 13409-1-AP; ProteinTech Group, Inc.), rabbit polyclonal Claudin-11 (1:500; cat. no. AF5364; Affinity Biosciences, OH, USA), rabbit polyclonal Claudin-5 (1:500; cat. no. AF5216; Affinity Biosciences), mouse monoclonal CHOP (L63F7) (1:1000; cat. no. 2895; Cell Signaling Technology, Shanghai, China), Rabbit polyclonal GRP78/BiP (1:1000; cat. No. ab21685; Abcam), rabbit polyclonal ATF4 (1:500; cat. no. 10835-1-AP; ProteinTech Group, Inc.), rabbit polyclonal ATF6 (1:500; cat. no. 24169-1-AP; ProteinTech Group, Inc.), rabbit polyclonal Calnexin (1:1000; cat. no. 10427-2-AP; ProteinTech Group, Inc.), rabbit polyclonal TMX1 (1:1000; cat. no. 27489-1-AP; ProteinTech Group, Inc.), rabbit polyclonal PDI (PDIA1) (1:500; cat. no. 11245-1-AP; ProteinTech Group, Inc.), rabbit polyclonal ERp57/ERp60 (PDIA3) (1:1000; cat. no. 15967-1-AP; ProteinTech Group, Inc.), mouse monoclonal β-actin (8H10D10) (1:1000; cat. no. 3700; Cell Signaling Technology). The secondary antibodies used include: goat anti-rabbit IgG (H + L) secondary antibody, horseradish peroxidase (HRP)-conjugated (1:5000; cat. no. 31460; Invitrogen; Thermo Fisher Scientific, Inc.) and goat anti-mouse IgG (H + L) secondary antibody, HRP-conjugated (1:5000; cat. no. 31430; Invitrogen; Thermo Fisher Scientific, Inc.). The proteins were visualized by BlodtightTM Western Chemiluminescent HRP Substrate (Bioworld, Visalia, CA, USA), and images were captured by Tanon-5200 Chemiluminescent Imaging System (Tanon Science and Technology, Co., Ltd., Shanghai, China). The intensities of bands were quantified using ImageJ version 1.32j software (National Institutes of Health, MD, USA).

4.17. Quantitative RT-PCR

The mRNA expression levels of ER stress-related genes were quantified using quantitative RT-PCR. Total RNA was extracted using a Total RNA Isolation Kit (BEI-BEI Biotech, Zhengzhou, China), and 1 μg total

RNA was then reverse-transcribed with PrimeScript RT Master Mix (Takara Bio, Inc., Otsu, Japan). For quantitative RT-PCR, transcripts were amplified using AceQ qPCR SYBR Green Master Mix (Vazyme Biotech, Nanjing, China), and fluorescence signals were monitored by a Roche LightCycler 96 Real-time PCR system (Roche Diagnostics, Basel, Switzerland). The gene 36B4 (ribosomal protein lateral stalk subunit P0) was used as an internal control, and the relative expression levels were figured up using the $2^{-\Delta\Delta Cq}$ method [68]. The sequences of the primers used in this study are listed in Table S4.

4.18. Fluorescent PA pulse-chase experiments and staining of organelles

PA endocytosis was detected using the fluorescence-labeled PA analogue, 4,4-difluoro-5,7-dimethyl-4-bora-3a,4a-diaza-*s*-indacene-3-hexadecanoic acid (BODIPY® FL C16; Thermo Fisher Scientific, Inc.) [69]. TM4 cells were incubated with 1 μM BODIPY® FL C16 diluted in DMEM/F12 for 0.5, 2, or 24 h. To localize organelles, we used Nile Red (Sigma-Aldrich), ER-Tracker Red (Beyotime), and MitoRed (KeyGEN BioTECH, Nanjing, China) to detect lipid droplets, the ER, and the mitochondria, respectively. Nuclei were stained with Hoechst 33,342 (Beyotime). Fluorescent images were captured using a Laser Scanning Confocal Microscope (LSM 710, Zeiss, Germany) equipped with a 40 × objective (for PA endocytosis tracing), or a High-Resolution Microscope (GE DeltaVision OMX, GE Healthcare, Little Chalfont, UK) equipped with a 60 × objective (for subcellular co-localization).

To observe ER structure and distribution, TM4 Sertoli cells were incubated with 10 μM ER-Tracker Green (Invitrogen; Thermo Fisher Scientific, Inc.) for 30 min, and the fluorescent images were captured using PerkinElmer Ultraview spinning disk confocal microscope equipped with a Nikon Apochromat TIRF 60 × 1.40NA objective and a Hamamatasu C9100–23B EMCCD camera. For sequential observation, fluorescent images were captured once per minute for 5 min, and the videos were produced using ImageJ version 1.32j software.

4.19. Detection of ROS generation

The generation of cytosolic ROS was detected using 2′, 7′ dichlorofluorescin diacetate (DCFH-DA). Mitochondrial ROS was detected by using MitoSOX to indicate mitochondrial superoxide. Briefly, after treatment, TM4 cells were loaded with 10 μM DCFH-DA (KeyGEN BioTECH, Nanjing, China) diluted in PBS for 30 min or 5 μM MitoSOX (Invitrogen; Thermo Fisher Scientific, Inc.) diluted in HBSS for 10 min at 37 °C. Then the cells were washed twice with PBS, and images were acquired on a fluorescence microscope (IX73; Olympus Corporation, Tokyo, Japan) equipped with a 20 × objective.

4.20. Detection of relative calcium (Ca^{2+}) concentration

Cytosolic Ca^{2+} indicator Fluo-3 and mitochondrial Ca^{2+} indicator Rhod-2 were used to stain TM4 Sertoil cells. In brief, after treatment, TM4 cells were incubated with 2 μM Fluo-3 (KeyGEN BioTECH) or 1 μM Rhod-2 (Abcam) diluted in phenol red-free DMEM/F12 medium for 30 min. Then the cells were washed twice with PBS, and images were acquired on a fluorescence microscope (IX73; Olympus Corporation, Tokyo, Japan) equipped with a 20 × objective.

4.21. Plasmid construction, RNAi and cell transfection

Plasmid over-expressing mouse C-terminally tagged Calnexin-Flag was generated by cloning the calnexin cDNA into pCDNA3.1 vector bearing the Flag tag. Constructs to express Calnexin with point mutations were constructed using Fast Site-Directed Mutagenesis Kit (TransGen Biotech Co., LTD, Beijing, China), following the manufacturer's instructions.

The siRNAs for CHOP and non-specific siRNA (negative control, NC) were designed and synthesized by Genepharma (Shanghai, China). The

sequences are as follows: siCHOP-1, 5′-GGAAGAGGAGGAAGAGCAA-3'; siCHOP-2, 5′-GCAAGGAAGAACUAGGAAA-3'; siCHOP-3, 5′-AGGA-GAAGGAGCAGGAGAA-3'.

For plasmid over-expression and RNAi, TM4 cells were transfected with plasmids or siRNAs using Lipofectamine 3000 reagent (Invitrogen; Thermo Fisher Scientific, Inc.) following the manufacturer's instructions. The following experiments were executed 24 h after the transfection.

4.22. ABE assay and mass spectrometry

Protein palmitoylation was analyzed using ABE assays as previously described with some modifications [70]. For total protein palmitoylation analysis, cells or testis samples were collected, and protein was extracted using RIPA Buffer (Sigma-Aldrich). Then the protein was incubated at 4 °C overnight with rotating in 50 mM N-ethylmaleimide (NEM, Sigma-Aldrich) diluted in RIPA Buffer. After precipitation with acetone, the protein samples were resuspended in 300 μl 4% SDS Buffer (4SB, containing 4% SDS, 50 mM Tris and 5 mM EDTA, pH 7.4), and each sample was divided into two equal parts (150 μl for each part): one part was mixed with 150 μl 1.5 M hydroxylamine solution (HA, Sigma-Aldrich) (+HA Sample), and the other part was mixed with 150 μl 0.1 M Tris-HCl (pH 7.4) (-HA Sample). After incubating at room temperature with rotating for 2 h, protein samples were precipitated with acetone, resuspended in 100 μl 4SB (pH6.2), mixed with 400 μl BMCC-Biotin Buffer (containing 6.25 μM BMCC-Biotin (Sangon, Shanghai, China), 150 mM NaCl, 50 mM Tris, 5 mM EDTA and 0.2% Triton X-100), and incubated with rotating for 2 h at room temperature. Finally, protein samples were precipitated with acetone again, and resuspended in appropriate volumes of 2% SDS Buffer (containing 2% SDS, 50 mM Tris and 5 mM EDTA, pH 7.4). Following quantification of protein concentrations using Pierce BCA protein analysis kit, 5 μg of each protein sample was resolved by polyacrylamide gel electrophoresis. Then, the proteins were transferred to polyvinylidene difluoride membranes, blocked, incubated with horseradish peroxidase-conjugated streptavidin (Beyotime), and visualized using BlodtightTM Western Chemiluminescent HRP Substrate. Images were captured by Tanon-5200 Chemiluminescent Imaging System.

For mass spectrometry analysis of palmitoylated proteins and the analysis of the palmitoylation levels of specific proteins, another method using HPDP-Biotin was executed. In brief, cells were collected after treatment, resuspended in lysis buffer, and lysed by ultrasonication. After centrifugation at 4 °C, 13,000×*g* to remove insoluble material, 2 mg of protein was taken out for each sample, and incubated at 4 °C overnight with rotating in 50 mM NEM. After precipitation with methanol/chloroform, the protein samples were resuspended in 200 μl resuspension buffer, and each sample was divided into two equal parts (100 μl for each part): one part was mixed with 800 μl 1 M HA, 1 mM EDTA, protease inhibitors and 100 μL 4 mM HPDP-Biotin (Thermo Scientific) (+HA Sample), and the other part was treated identically but HA was replaced with 50 mM Tris (pH 7.4) (-HA Sample). After incubating at room temperature with rotating for 2 h, protein samples were precipitated with methanol/chloroform, resuspended in 100 μl resuspension buffer, and added with 900 μl PBS containing 0.2% Triton X-100. In each sample, 50 μl was removed as a loading control, and the remaining was incubated with 15 μl streptavidin-agarose beads (Thermo scientific) for 2 h at room temperature. The beads were washed twice with wash buffer, and 3–5 times with PBS. Finally, the beads were resuspended with 25 μL 2 × SDS sample buffer containing 1% 2-mercaptoethanol v/v, and proteins were eluted by heating at 95 °C for 5 min. Samples were analyzed by Western blotting.

For mass spectrometry, palmitoylated proteins (100 μg) extracted and purified from each sample were reduced by DTT and carboxyamidomethylated by iodoacetamide. After digestion with trypsin, the peptide mixtures were desalted, freeze dried and then resuspended in buffer A (2% ACN, 0.1% FA). The resuspended samples were centrifuged

at 20,000×*g* for 10 min, and the supernatants were collected and loaded on a LC-20AD nano-HPLC (Shimadzu, Kyoto, Japan) by the autosampler onto a C18 trap column (inner diameter 75 μm), followed by a gradient separation. The column outlet was coupled directly to nanoelectrospray ionization (nanoESI) tandem mass spectrometry (Q-Exactive, Thermo Fisher Scientific, San Jose,CA), and analyzed using DDA (Data-Dependent Acquisition) method. Protein identification was performed with MaxQuant integrated Andromeda search engine against the UniProt *Mus musculus* protein database (17,015 sequences). The analysis was performed by Beijing Genomics Institution. The mass spectrometry proteomics data have been deposited to the ProteomeXchange Consortium via the PRIDE [71] partner repository with the dataset identifier PXD028778.

4.23. Statistical analyses

Data were plotted using GraphPad Prism 8 (GraphPad Software Inc., LA Jolla, CA, USA), and are presented as means ± standard deviation (SD). Different groups were compared using one-way analyses of variance followed by least significant difference (equal variances) or Games-Howell (unequal variances) post-hoc tests, using SPSS Software Version 17.0 (SPSS, Inc., Chicago, Illinois, USA). Values with $p < 0.05$ were regarded as significantly different.

Data availability

The mass spectrometry proteomics data have been deposited to the ProteomeXchange Consortium via the PRIDE [71] partner repository with the dataset identifier PXD028778. The datasets generated during and/or analyzed during the current study are available from the corresponding author on reasonable request.

Ethics approval

All procedures followed were in accordance with the ethical standards of the responsible committee on human experimentation (the Dermatology Hospital of Southern Medical University) and with the Helsinki Declaration of 1975, as revised in 2000. Informed consent was obtained from all patients for being included in the study. All institutional and national guidelines for the care and use of laboratory animals were followed.

Author contribution

B. Y., X. G., N. S. and C. F. designed and coordinated the whole study. X. G., Z. H. and C. C. conducted most *in vitro* and *in vivo* assay. T. X. and L.L. provided technical assistance and participated in palmitoylated protein analysis. J. J., Y. F. and Z. Z. collected clinical samples. R. M. and W. Z. participated in animal experiments. K. J. and J. M. participated in cell experiments. J. J., Z. Q. and L. C. contributed to data calibration. X. G., Z. H. and C. C. analyzed the data. X. G. and B. Y. wrote the manuscript.

Declaration of competing interest

The authors declare that they have no known competing financial interests or personal relationships that could have appeared to influence the work reported in this paper.

Appendix A. Supplementary data

Supplementary data to this article can be found online at https://doi.org/10.1016/j.redox.2022.102380.

Abbreviations:

2-BP	2-bromopalmitate
4SB	4% SDS Buffer
ABE	acyl-biotin exchange
Atf4	activating transcription factor 4
BTB	blood-testis barrier
Chop	C/EBP homologous protein
CLDN5	claudin 5
CLDN11	claudin 11
CNX	Calnexin
COG	Cluster of Orthologous Groups of proteins
Edem	ER degradation-enhancing alpha-mannosidase like protein 1
EO	extreme oligospermia
ER	endoplasmic reticulum
FBS	fetal bovine serum
FITC-I	fluorescein isothiocyanate isomer I
FSH	follicle-stimulating hormone
Gadd34	growth arrest and DNA damage-inducible transcript 34
GC/MS	gas chromatography coupled to mass spectrometry
GO	Gene Ontology
Grp78	glucose-regulated protein 78
HA	hydroxylamine solution
Herpud1	homocysteine-inducible endoplasmic reticulum stress-inducible ubiquitin-like domain member 1 protein
Hyou1	hypoxia upregulated 1
INHB	inhibin B
IRE1	inositol-requiring enzyme 1
LH	luteinizing hormone
MLCFA	medium and long-chain fatty acid
NEM	N-ethylmaleimide
NOA	non-obstructive azoospermia
OCLN	occludin
P4hb/PDIA1/ERP59	prolyl 4-hydroxylase, beta polypeptide
PA	palmitic acid
PDIA3/ERP57	protein disulfide-isomerase A3 precursor
PERK	protein kinase R-like endoplasmic reticulum kinase
PUFA	polyunsaturated fatty acid
RNAi	RNA interfering
ROS	reactive oxygen species
SD	standard deviation
SFA	saturated fatty acid
siRNA	short interfering RNA
T	testosterone
TER	transepithelial resistance
TM	tunicamycin
TMX1	thioredoxin related transmembrane protein 1

USFA   unsaturated fatty acid
Xbp1   X-box binding protein 1
ZO-1   zona occluden-1

References

[1] E.P.P. Evans, J.T.M. Scholten, A. Mzyk, C. Reyes-San-Martin, A.E. Llumbet, T. Hamoh, E. Arts, R. Schirhagl, A.E.P. Cantineau, Male subfertility and oxidative stress, Redox Biol. 46 (2021), 102071, https://doi.org/10.1016/j.redox.2021.102071.

[2] P.S. Deshpande, A.S. Gupta, Causes and prevalence of factors causing infertility in a public Health facility, J. Hum. Reprod. Sci. 12 (4) (2019) 287–293, https://doi.org/10.4103/jhrs.JHRS_140_18.

[3] M.J. McCabe, G.A. Tarulli, G. Laven-Law, K.L. Matthiesson, S.J. Meachem, R.I. McLachlan, M.E. Dinger, P.G. Stanton, Gonadotropin suppression in men leads to a reduction in claudin-11 at the Sertoli cell tight junction, Hum. Reprod. 31 (4) (2016) 875–886, https://doi.org/10.1093/humrep/dew009 dew009 [pii].

[4] R. Zhu, J. Wang, T. Feng, X. Hu, C. Jiang, X. Wang, K. Li, Y. Sang, Y. Hua, H. Sun, B. Yao, C. Li, The alteration of RhoA geranylgeranylation and Ras farnesylation breaks the integrity of the blood-testis barrier and results in hypospermatogenesis, Cell Death Dis. 10 (6) (2019) 450, https://doi.org/10.1038/s41419-019-1688-9.

[5] C.D. Morrison, R.E. Brannigan, Metabolic syndrome and infertility in men, Best Pract. Res. Clin. Obstet. Gynaecol. 29 (4) (2015) 507–515, https://doi.org/10.1016/j.bpobgyn.2014.10.006.

[6] Y. Fan, Y. Liu, K. Xue, G. Gu, W. Fan, Y. Xu, Z. Ding, Diet-induced obesity in male C57BL/6 mice decreases fertility as a consequence of disrupted blood-testis barrier, PLoS One 10 (4) (2015), e0120775, https://doi.org/10.1371/journal.pone.0120775 PONE-D-14-43799 [pii].

[7] J. Bermudez-Cardona, C. Velasquez-Rodriguez, Profile of free fatty acids and fractions of phospholipids, cholesterol esters and triglycerides in serum of obese youth with and without metabolic syndrome, Nutrients 8 (2) (2016) 54, https://doi.org/10.3390/nu8020054 E54 [pii] nu8020054 [pii].

[8] J. Staaf, S.J. Ubhayasekera, E. Sargsyan, A. Chowdhury, H. Kristinsson, H. Manell, J. Bergquist, A. Forslund, P. Bergsten, Initial hyperinsulinemia and subsequent beta-cell dysfunction is associated with elevated palmitate levels, Pediatr. Res. 80 (2) (2016) 267–274, https://doi.org/10.1038/pr.2016.80 pr201680 [pii].

[9] X. Hu, X. Ge, W. Liang, Y. Shao, J. Jing, C. Wang, R. Zeng, B. Yao, Effects of saturated palmitic acid and omega-3 polyunsaturated fatty acids on Sertoli cell apoptosis, Syst. Biol. Reprod. Med. 64 (5) (2018) 368–380, https://doi.org/10.1080/19396368.2018.1471554.

[10] X. Ge, P. Pan, J. Jing, X. Hu, L. Chen, X. Qiu, R. Ma, K. Jueraitetibaike, X. Huang, B. Yao, Rosiglitazone ameliorates palmitic acid-induced cytotoxicity in TM4 Sertoli cells, Reprod. Biol. Endocrinol. 16 (1) (2018) 98, https://doi.org/10.1186/s12958-018-0416-0 10.1186/s12958-018-0416-0 [pii].

[11] O. Ramos-Lopez, J.I. Riezu-Boj, F.I. Milagro, M.J. Moreno-Aliaga, J.A. Martinez, Endoplasmic reticulum stress epigenetics is related to adiposity, dyslipidemia, and insulin resistance, Adipocyte 7 (2) (2018) 137–142, https://doi.org/10.1080/21623945.2018.1447731.

[12] S.G. Chu, J.A. Villalba, X. Liang, K. Xiong, K. Tsoyi, B. Ith, E.A. Ayaub, R.V. Tatituri, D.E. Byers, F.F. Hsu, S. El-Chemaly, E.Y. Kim, Y. Shi, I.O. Rosas, Palmitic acid-rich high-fat diet exacerbates experimental pulmonary fibrosis by modulating endoplasmic reticulum stress, Am. J. Respir. Cell Mol. Biol. 61 (6) (2019) 737–746, https://doi.org/10.1165/rcmb.2018-0324OC.

[13] S.S. Cao, R.J. Kaufman, Endoplasmic reticulum stress and oxidative stress in cell fate decision and human disease, Antioxidants Redox Signal. 21 (3) (2014) 396–413, https://doi.org/10.1089/ars.2014.5851.

[14] S.H. Seo, S.E. Kim, S.E. Lee, ER stress induced by ER calcium depletion and UVB irradiation regulates tight junction barrier integrity in human keratinocytes, J. Dermatol. Sci. 98 (1) (2020) 41–49, https://doi.org/10.1016/j.jdermsci.2020.02.006.

[15] M.J. Pagliassotti, P.Y. Kim, A.L. Estrada, C.M. Stewart, C.L. Gentile, Endoplasmic reticulum stress in obesity and obesity-related disorders: an expanded view, Metabolism 65 (9) (2016) 1238–1246, https://doi.org/10.1016/j.metabol.2016.05.002 S0026-0495(16)30017-8 [pii].

[16] G.L. Vilas, L.G. Berthiaume, A role for palmitoylation in the quality control, assembly and secretion of apolipoprotein B, Biochem. J. 377 (Pt 1) (2004) 121–130, https://doi.org/10.1042/BJ20030951 BJ20030951 [pii].

[17] E.M. Lynes, M. Bui, M.C. Yap, M.D. Benson, B. Schneider, L. Ellgaard, L.G. Berthiaume, T. Simmen, Palmitoylated TMX and calnexin target to the mitochondria-associated membrane, EMBO J. 31 (2) (2012) 457–470, https://doi.org/10.1038/emboj.2011.384 emboj2011384 [pii].

[18] M. Jiang, J. Hu, F.K.H. White, J. Williamson, A.S. Klymchenko, A. Murthy, S.W. Workman, G.N. Tseng, S-Palmitoylation of junctophilin-2 is critical for its role in tethering the sarcoplasmic reticulum to the plasma membrane, J. Biol. Chem. 294 (36) (2019) 13487–13501, https://doi.org/10.1074/jbc.RA118.006772 RA118.006772 ([pii]).

[19] Z. Pei, Y. Xiao, J. Meng, A. Hudmon, T.R. Cummins, Cardiac sodium channel palmitoylation regulates channel availability and myocyte excitability with implications for arrhythmia generation, Nat. Commun. 7 (2016), 12035, https://doi.org/10.1038/ncomms12035 ncomms12035 [pii].

[20] G. Carta, E. Murru, S. Banni, C. Manca, Palmitic acid: physiological role, metabolism and nutritional implications, Front. Physiol. 8 (2017) 902, https://doi.org/10.3389/fphys.2017.00902.

[21] C.L. Jackson, Lipid droplet biogenesis, Curr. Opin. Cell Biol. 59 (2019) 88–96, https://doi.org/10.1016/j.ceb.2019.03.018, https://doi.org/S0955-0674(18)30137-6 [pii].

[22] H.M. Zeeshan, G.H. Lee, H.R. Kim, H.J. Chae, Endoplasmic reticulum stress and associated ROS, Int. J. Mol. Sci. 17 (3) (2016) 327, https://doi.org/10.3390/ijms17030327.

[23] S. Wakabayashi, H. Yoshida, The essential biology of the endoplasmic reticulum stress response for structural and computational biologists, Comput. Struct. Biotechnol. J. 6 (2013), e201303010, https://doi.org/10.5936/csbj.201303010 CSBJ-6-e201303010 [pii].

[24] S. Wang, Z. Qian, X. Ge, C. Li, M. Xue, K. Liang, R. Ma, L. Ouyang, L. Zheng, J. Jing, S. Cao, Y. Zhang, Y. Yang, Y. Chen, J. Ma, B. Yao, LncRNA Tug 1 maintains blood-testis barrier integrity by modulating Ccl2 expression in high-fat diet mice, Cell. Mol. Life Sci. 79 (2) (2022) 114, https://doi.org/10.1007/s00018-022-04142-3.

[25] Y. Li, Y. Guo, J. Tang, J. Jiang, Z. Chen, New insights into the roles of CHOP-induced apoptosis in ER stress, Acta Biochim. Biophys. Sin. 47 (2) (2015) 146–147, https://doi.org/10.1093/abbs/gmu128.

[26] A.K. Lakkaraju, L. Abrami, T. Lemmin, S. Blaskovic, B. Kunz, A. Kihara, M. Dal Peraro, F.G. van der Goot, Palmitoylated calnexin is a key component of the ribosome-translocon complex, EMBO J. 31 (7) (2012) 1823–1835, https://doi.org/10.1038/emboj.2012.15.

[27] E.M. Lynes, A. Raturi, M. Shenkman, C. Ortiz Sandoval, M.C. Yap, J. Wu, A. Janowicz, N. Myhill, M.D. Benson, R.E. Campbell, L.G. Berthiaume, G.Z. Lederkremer, T. Simmen, Palmitoylation is the switch that assigns calnexin to quality control or ER Ca2+ signaling, J. Cell Sci. 126 (Pt 17) (2013) 3893–3903, https://doi.org/10.1242/jcs.125856.

[28] W. Stoffel, I. Schmidt-Soltau, E. Binczek, A. Thomas, M. Thevis, I. Wegner, Dietary ω3-and ω6-Polyunsaturated fatty acids reconstitute fertility of Juvenile and adult Fads2-Deficient mice, Mol. Metabol. 36 (2020), 100974, https://doi.org/10.1016/j.molmet.2020.100974.

[29] A.C. Skulas-Ray, P.W.F. Wilson, W.S. Harris, E.A. Brinton, P.M. Kris-Etherton, C.K. Richter, T.A. Jacobson, M.B. Engler, M. Miller, J.G. Robinson, C.B. Blum, D. Rodriguez-Leyva, S.D. de Ferranti, F.K. Welty, Omega-3 fatty acids for the management of hypertriglyceridemia: a science advisory from the American heart association, Circulation 140 (12) (2019) e673–e691, https://doi.org/10.1161/cir.0000000000000709.

[30] K. Shiraishi, H. Matsuyama, Effects of medical comorbidity on male infertility and comorbidity treatment on spermatogenesis, Fertil. Steril. 110 (6) (2018) 1006–1011, https://doi.org/10.1016/j.fertnstert.2018.07.002, e2.

[31] G. Eslamian, N. Amirjannati, B. Rashidkhani, M.R. Sadeghi, A.R. Baghestani, A. Hekmatdoost, Dietary fatty acid intakes and asthenozoospermia: a case-control study, Fertil. Steril. 103 (1) (2015) 190–198.

[32] A. Khosrowbeygi, N. Zarghami, Fatty acid composition of human spermatozoa and seminal plasma levels of oxidative stress biomarkers in subfertile males, Prostaglandins Leukot. Essent. Fatty Acids 77 (2) (2007) 117–121, https://doi.org/10.1016/j.plefa.2007.08.003, https://doi.org/S0952-3278(07)00103-2 [pii].

[33] F. Nasrallah, S.H. Taieb, M.M. Sethoum, S. Omar, H.B. Aribia, H. Sanhaji, M. Feki, Altered semen quality is associated with decreased semen docosahexaenoic acid and increased oleic acid levels, Clin. Lab. 66 (1) (2020), https://doi.org/10.7754/Clin.Lab.2019.190515.

[34] B. Tang, X. Shang, H. Qi, J. Li, B. Ma, G. An, Q. Zhang, Metabonomic analysis of fatty acids in seminal plasma between healthy and asthenozoospermic men based on gas chromatography mass spectrometry, Andrologia 49 (9) (2017), https://doi.org/10.1111/and.12744.

[35] X. Hu, Z. Ding, Z. Hong, Z. Zou, Y. Feng, R. Zhu, J. Ma, X. Ge, C. Li, B. Yao, Spermatogenesis improved by suppressing the high level of endogenous gonadotropins in idiopathic non-obstructive azoospermia: a case control pilot study, Reprod. Biol. Endocrinol. 16 (1) (2018) 91, https://doi.org/10.1186/s12958-018-0401-7 10.1186/s12958-018-0401-7 [pii].

[36] D. Xu, L. Liu, Y. Zhao, L. Yang, J. Cheng, R. Hua, Z. Zhang, Q. Li, Melatonin protects mouse testes from palmitic acid-induced lipotoxicity by attenuating oxidative stress and DNA damage in a SIRT1-dependent manner, J. Pineal Res. 6 (10) (2020), 12690.

[37] I.L. Lemmer, N. Willemsen, N. Hilal, A. Bartelt, A guide to understanding endoplasmic reticulum stress in metabolic disorders, Mol. Metabol. 47 (2021), 101169, https://doi.org/10.1016/j.molmet.2021.101169.

[38] T. Dolinay, B.E. Himes, M. Shumyatcher, G.G. Lawrence, S.S. Margulies, Integrated stress response mediates epithelial injury in mechanical ventilation, Am. J. Respir. Cell Mol. Biol. 57 (2) (2017) 193–203, https://doi.org/10.1165/rcmb.2016-0404OC.

[39] W.A. Cabral, M. Ishikawa, M. Garten, E.N. Makareeva, B.M. Sargent, M. Weis, A.M. Barnes, E.A. Webb, N.J. Shaw, L. Ala-Kokko, F.L. Lacbawan, W. Hogler, S. Leikin, P.S. Blank, J. Zimmerberg, D.R. Eyre, Y. Yamada, J.C. Marini, Absence of the ER cation channel TMEM38B/TRIC-B disrupts intracellular calcium homeostasis and dysregulates collagen synthesis in recessive osteogenesis imperfecta, PLoS Genet. 12 (7) (2016), e1006156, https://doi.org/10.1371/journal.pgen.1006156.

[40] Y.H. Hsiao, C.I. Lin, H. Liao, Y.H. Chen, S.H. Lin, Palmitic acid-induced neuron cell cycle G2/M arrest and endoplasmic reticular stress through protein palmitoylation in SH-SY5Y human neuroblastoma cells, Int. J. Mol. Sci. 15 (11) (2014) 20876–20899, https://doi.org/10.3390/ijms151120876 ijms151120876 [pii].

[41] A.C. Baldwin, C.D. Green, L.K. Olson, M.A. Moxley, J.A. Corbett, A role for aberrant protein palmitoylation in FFA-induced ER stress and beta-cell death, Am. J. Physiol. Endocrinol. Metab. 302 (11) (2012) E1390–E1398, https://doi.org/10.1152/ajpendo.00519.2011 ajpendo.00519.2011 ([pii]).

[42] Y. Yu, R. Guo, Y. Zhang, H. Shi, H. Sun, X. Chu, X. Wu, H. Lu, C. Sun, miRNA-mRNA profile and regulatory network in stearic acid-treated beta-cell dysfunction, J. Endocrinol. 246 (1) (2020) 13–27, https://doi.org/10.1530/JOE-20-0055.

[43] V. Esmaeili, A.H. Shahverdi, M.H. Moghadasian, A.R. Alizadeh, Dietary fatty acids affect semen quality: a review, Andrology 3 (3) (2015) 450–461, https://doi.org/10.1111/andr.12024.

[44] K. Essandoh, J.M. Philippe, P.M. Jenkins, M.J. Brody, Palmitoylation: a fatty regulator of myocardial electrophysiology, Front. Physiol. 11 (2020) 108, https://doi.org/10.3389/fphys.2020.00108.

[45] Y. Cao, M. Fan, Y. Pei, L. Su, W. Xiao, F. Chen, J. Huang, X. Liu, Z. Gu, Z. Zhang, F. Yuan, Y. Jiang, X. Han, CCAAT/Enhancer-Binding protein homologous protein (CHOP) deficiency attenuates heatstroke-induced intestinal injury, Inflammation 45 (2) (2022) 695–711, https://doi.org/10.1007/s10753-021-01577-x.

[46] Y. Fan, T. Simmen, Mechanistic connections between endoplasmic reticulum (ER) redox control and mitochondrial metabolism, Cells 8 (9) (2019), https://doi.org/10.3390/cells8091071.

[47] N. Bousette, C. Abbasi, R. Chis, A.O. Gramolini, Calnexin silencing in mouse neonatal cardiomyocytes induces Ca2+ cycling defects, ER stress, and apoptosis, J. Cell. Physiol. 229 (3) (2014) 374–383, https://doi.org/10.1002/jcp.24459.

[48] T. Paskevicius, J. Jung, M. Pujol, P. Eggleton, W. Qin, A. Robinson, N. Gutowski, J. Holley, M. Smallwood, J. Newcombe, D. Zochodne, X.Z. Chen, J. Tang, A. Kraus, M. Michalak, L.B. Agellon, The Fabp5/calnexin complex is a prerequisite for sensitization of mice to experimental autoimmune encephalomyelitis, Faseb. J. 34 (12) (2020) 16662–16675, https://doi.org/10.1096/fj.202001539RR.

[49] T. Lan, C. Delalande, B.C. Dickinson, Inhibitors of DHHC family proteins, Curr. Opin. Chem. Biol. 65 (2021) 118–125, https://doi.org/10.1016/j.cbpa.2021.07.002.

[50] Y. Webb, L. Hermida-Matsumoto, M.D. Resh, Inhibition of protein palmitoylation, raft localization, and T cell signaling by 2-bromopalmitate and polyunsaturated fatty acids, J. Biol. Chem. 275 (1) (2000) 261–270, https://doi.org/10.1074/jbc.275.1.261.

[51] E. Thinon, A. Percher, H.C. Hang, Bioorthogonal chemical reporters for monitoring unsaturated fatty-acylated proteins, Chembiochem 17 (19) (2016) 1800–1803, https://doi.org/10.1002/cbic.201600213.

[52] J. Schulte-Zweckel, M. Dwivedi, A. Brockmeyer, P. Janning, R. Winter, G. Triola, A hydroxylamine probe for profiling S-acylated fatty acids on proteins, Chem. Commun. 55 (75) (2019) 11183–11186, https://doi.org/10.1039/c9cc05989j.

[53] T. Anusornvongchai, M. Nangaku, T.M. Jao, C.H. Wu, Y. Ishimoto, H. Maekawa, T. Tanaka, A. Shimizu, M. Yamamoto, N. Suzuki, R. Sassa, R. Inagi, Palmitate deranges erythropoietin production via transcription factor ATF4 activation of unfolded protein response, Kidney Int. 94 (3) (2018) 536–550, https://doi.org/10.1016/j.kint.2018.03.011.

[54] H. Yao, J. Lan, C. Li, H. Shi, J.P. Brosseau, H. Wang, H. Lu, C. Fang, Y. Zhang, L. Liang, X. Zhou, C. Wang, Y. Xue, Y. Cui, J. Xu, Inhibiting PD-L1 palmitoylation enhances T-cell immune responses against tumours, Nat Biomed Eng 3 (4) (2019) 306–317, https://doi.org/10.1038/s41551-019-0375-6.

[55] A.R. Martins, A.R. Crisma, L.N. Masi, C.L. Amaral, G.N. Marzuca-Nassr, L.H. M. Bomfim, B.G. Teodoro, A.L. Queiroz, T.D.A. Serdan, R.P. Torres, J. Mancini-Filho, A.C. Rodrigues, T.C. Alba-Loureiro, T.C. Pithon-Curi, R. Gorjao, L.R. Silveira, R. Curi, P. Newsholme, S.M. Hirabara, Attenuation of obesity and insulin resistance by fish oil supplementation is associated with improved skeletal muscle mitochondrial function in mice fed a high-fat diet, J. Nutr. Biochem. 55 (2018) 76–88, https://doi.org/10.1016/j.jnutbio.2017.11.012.

[56] J. Jing, N. Ding, D. Wang, X. Ge, J. Ma, R. Ma, X. Huang, K. Jueraitetibaike, K. Liang, S. Wang, S. Cao, A.Z. Zhao, B. Yao, Oxidized-LDL inhibits testosterone biosynthesis by affecting mitochondrial function and the p38 MAPK/COX-2 signaling pathway in Leydig cells, Cell Death Dis. 11 (8) (2020) 626, https://doi.org/10.1038/s41419-020-02751-z.

[57] E.W. Wong, W.M. Lee, C.Y. Cheng, Secreted Frizzled-related protein 1 (sFRP1) regulates spermatid adhesion in the testis via dephosphorylation of focal adhesion kinase and the nectin-3 adhesion protein complex, Faseb. J. 27 (2) (2013) 464–477, https://doi.org/10.1096/fj.12-212514.

[58] T. Fullston, E.M. Ohlsson-Teague, C.G. Print, L.Y. Sandeman, M. Lane, Sperm microRNA content is altered in a mouse model of male obesity, but the same suite of microRNAs are not altered in offspring's sperm, PLoS One 11 (11) (2016), e0166076, https://doi.org/10.1371/journal.pone.0166076.

[59] F. Paillard, D. Catheline, F.L. Duff, M. Bouriel, Y. Deugnier, M. Pouchard, J. C. Daubert, P. Legrand, Plasma palmitoleic acid, a product of stearoyl-coA desaturase activity, is an independent marker of triglyceridemia and abdominal adiposity, Nutr. Metabol. Cardiovasc. Dis. 18 (6) (2008) 436–440, https://doi.org/10.1016/j.numecd.2007.02.017, https://doi.org/S0939-4753(07)00087-7 [pii].

[60] Y. Shen, Z. Zhao, L. Zhang, L. Shi, S. Shahriar, R.B. Chan, G. Di Paolo, W. Min, Metabolic activity induces membrane phase separation in endoplasmic reticulum, Proc. Natl. Acad. Sci. U. S. A. 114 (51) (2017) 13394–13399, https://doi.org/10.1073/pnas.1712555114.

[61] A.K. Leamy, R.A. Egnatchik, M. Shiota, P.T. Ivanova, D.S. Myers, H.A. Brown, J. D. Young, Enhanced synthesis of saturated phospholipids is associated with ER stress and lipotoxicity in palmitate treated hepatic cells, J. Lipid Res. 55 (7) (2014) 1478–1488, https://doi.org/10.1194/jlr.M050237 jlr.M050237 ([pii]).

[62] P. Zhang, P.X. Wang, L.P. Zhao, X. Zhang, Y.X. Ji, X.J. Zhang, C. Fang, Y.X. Lu, X. Yang, M.M. Gao, Y. Zhang, S. Tian, X.Y. Zhu, J. Gong, X.L. Ma, F. Li, Z. Wang, Z. Huang, Z.G. She, H. Li, The deubiquitinating enzyme TNFAIP3 mediates inactivation of hepatic ASK1 and ameliorates nonalcoholic steatohepatitis, Nat. Med. 24 (1) (2018) 84–94, https://doi.org/10.1038/nm.4453.

[63] R. Fan, A. Toubal, S. Goni, K. Drareni, Z. Huang, F. Alzaid, R. Ballaire, P. Ancel, N. Liang, A. Damdimopoulos, I. Hainault, A. Soprani, J. Aron-Wisnewsky, F. Foufelle, T. Lawrence, J.F. Gautier, N. Venteclef, E. Treuter, Loss of the co-repressor GPS2 sensitizes macrophage activation upon metabolic stress induced by obesity and type 2 diabetes, Nat. Med. 22 (7) (2016) 780–791, https://doi.org/10.1038/nm.4114.

[64] M.R. Sam, M. Tavakoli-Mehr, R. Safaralizadeh, Omega-3 fatty acid DHA modulates p53, survivin, and microRNA-16-1 expression in KRAS-mutant colorectal cancer stem-like cells, Genes Nutr 13 (2018) 8, https://doi.org/10.1186/s12263-018-0596-4.

[65] A. Taha, F. Sharifpanah, M. Wartenberg, H. Sauer, Omega-3 and Omega-6 polyunsaturated fatty acids stimulate vascular differentiation of mouse embryonic stem cells, J. Cell. Physiol. 235 (10) (2020) 7094–7106, https://doi.org/10.1002/jcp.29606.

[66] Y. Zhang, H. Chen, W. Zhang, Y. Cai, P. Shan, D. Wu, B. Zhang, H. Liu, Z.A. Khan, G. Liang, Arachidonic acid inhibits inflammatory responses by binding to myeloid differentiation factor-2 (MD2) and preventing MD2/toll-like receptor 4 signaling activation, Biochim. Biophys. Acta, Mol. Basis Dis. 1866 (5) (2020), 165683, https://doi.org/10.1016/j.bbadis.2020.165683.

[67] X. Ge, S.Y. Chen, M. Liu, T.M. Liang, C. Liu, Evodiamine inhibits PDGFBBinduced proliferation of rat vascular smooth muscle cells through the suppression of cell cycle progression and oxidative stress, Mol. Med. Rep. 14 (5) (2016) 4551–4558, https://doi.org/10.3892/mmr.2016.5798.

[68] K.J. Livak, T.D. Schmittgen, Analysis of relative gene expression data using real-time quantitative PCR and the 2(-Delta Delta C(T)) Method, Methods 25 (4) (2001) 402–408, https://doi.org/10.1006/meth.2001.1262 S1046-2023(01)91262-9 [pii].

[69] H.G. Cheon, Y.S. Cho, Protection of palmitic acid-mediated lipotoxicity by arachidonic acid via channeling of palmitic acid into triglycerides in C2C12, J. Biomed. Sci. 21 (2014) 13, https://doi.org/10.1186/1423-0127-21-13 1423-0127-21-13 ([pii]).

[70] J. Wan, A.F. Roth, A.O. Bailey, N.G. Davis, Palmitoylated proteins: purification and identification, Nat. Protoc. 2 (7) (2007) 1573–1584, https://doi.org/10.1038/nprot.2007.225.

[71] Y. Perez-Riverol, A. Csordas, J. Bai, M. Bernal-Llinares, S. Hewapathirana, D. J. Kundu, A. Inuganti, J. Griss, G. Mayer, M. Eisenacher, E. Pérez, J. Uszkoreit, J. Pfeuffer, T. Sachsenberg, S. Yilmaz, S. Tiwary, J. Cox, E. Audain, M. Walzer, A. F. Jarnuczak, T. Ternent, A. Brazma, J.A. Vizcaíno, The PRIDE database and related tools and resources in 2019: improving support for quantification data, Nucleic Acids Res. 47 (D1) (2019) D442–D450, https://doi.org/10.1093/nar/gky1106.